UC San Diego
UC San Diego Previously Published Works

Title

Measurement of associated Z + charm production in proton—proton collisions at s=8TeV

Permalink

https://escholarship.org/uc/item/52b0j14s

Journal

European Physical Journal C, 78(4)

ISSN

1434-6044

Authors

Sirunyan, AM

Tumasyan, A

Adam, W

et al.

Publication Date

2018-04-01

DOI

10.1140/epjc/s10052-018-5752-x

Copyright Information

Peer reviewed

THE EUROPEAN
PHYSICAL JOURNAL C

CrossMark

Measurement of associated Z + charm production in proton–proton collisions at $\sqrt{s} = 8\,\mathrm{TeV}$

CMS Collaboration[*]

CERN, 1211 Geneva 23, Switzerland

Abstract A study of the associated production of a Z boson and a charm quark jet (Z + c), and a comparison to production with a b quark jet (Z + b), in pp collisions at a centre-of-mass energy of 8 TeV are presented. The analysis uses a data sample corresponding to an integrated luminosity of 19.7 fb^{-1}, collected with the CMS detector at the CERN LHC. The Z boson candidates are identified through their decays into pairs of electrons or muons. Jets originating from heavy flavour quarks are identified using semileptonic decays of c or b flavoured hadrons and hadronic decays of charm hadrons. The measurements are performed in the kinematic region with two leptons with $p_T^\ell > 20\,\mathrm{GeV}$, $|\eta^\ell| < 2.1$, $71 < m_{\ell\ell} < 111\,\mathrm{GeV}$, and heavy flavour jets with $p_T^{\mathrm{jet}} > 25\,\mathrm{GeV}$ and $|\eta^{\mathrm{jet}}| < 2.5$. The Z + c production cross section is measured to be $\sigma(\mathrm{pp} \to \mathrm{Z}+\mathrm{c}+X)\mathcal{B}(\mathrm{Z} \to \ell^+\ell^-) = 8.8\pm0.5\,(\mathrm{stat})\pm0.6\,(\mathrm{syst})$ pb. The ratio of the Z+c and Z+b production cross sections is measured to be $\sigma(\mathrm{pp} \to \mathrm{Z}+\mathrm{c}+X)/\sigma(\mathrm{pp} \to \mathrm{Z}+\mathrm{b}+X) = 2.0\pm0.2\,(\mathrm{stat})\pm0.2\,(\mathrm{syst})$. The Z+c production cross section and the cross section ratio are also measured as a function of the transverse momentum of the Z boson and of the heavy flavour jet. The measurements are compared with theoretical predictions.

1 Introduction

The CERN Large Hadron Collider (LHC) has delivered a large sample of pp collisions containing events with a vector boson (V) accompanied by one or more jets (V+jets). Some of these events involve the production of a vector boson in association with jets originating from heavy flavour (HF) quarks and can be used to study specific predictions of the standard model (SM).

These V+jets events constitute an important background to many ongoing searches for new physics beyond the SM. A proper characterization of these processes and validation of their theoretical description is important to provide a reliable estimate of their specific backgrounds to the various searches. For example, third-generation scalar quarks (squarks) that are predicted by supersymmetric theories to decay via charm quarks have been searched for in final states with a charm quark jet (c jet) and a large transverse momentum imbalance [1–3]. A dominant background to this process is the associated production of a c jet and a Z boson that decays invisibly into neutrinos. An improved description of this background can be obtained from a measurement of the same process with the Z boson decaying into charged leptons.

Similarly, the associated production of a Z boson and HF jets is a significant background to the production of the Higgs boson in association with a Z boson (pp $\to$ Z+H+X; H $\to$ q$\bar{\mathrm{q}}$). Experimental studies of this process in the context of the SM focus on an analysis with b quarks in the final state [4–7], although some models beyond the SM also predict enhanced decay rates in the c$\bar{\mathrm{c}}$ final state [8]. In either case, it is important to understand the relative contribution of the different flavours to the Z+HF jets background to minimize the associated systematic uncertainties.

The possibility of observing evidence of an intrinsic charm (IC) quark component in the nucleon has recently received renewed interest [9]. The associated production of neutral vector bosons and c jets (V+c) has been identified [10–13] as a suitable process to investigate this physics topic. One of the main effects of an IC component would be an enhancement of Z+c production, mainly at large values of the transverse momentum of the Z boson and of the c jet.

Production of a Z boson and a c jet has been studied in high-energy hadron collisions by the D0 [14] and CDF [15] experiments at the Tevatron p$\bar{\mathrm{p}}$ collider. More recently, the LHCb Collaboration has measured the associated production of a Z boson and a D meson in the forward region in pp collisions at $\sqrt{s} = 7\,\mathrm{TeV}$ [16].

In this paper we present a measurement of the production cross section at $\sqrt{s} = 8\,\mathrm{TeV}$ of a Z boson and at least one jet from a c quark. In addition, the relative production of a Z

[*] e-mail: cms-publication-committee-chair@cern.ch

boson and a jet from heavy quarks of different flavours (c or b) is quantified by the ratio of their production cross sections. The associated production of a Z boson and at least one or two b jets using an inclusive b tagging technique to identify Z+b events has been studied with the same dataset and the results are reported in Ref. [17]. To reduce the uncertainties in the ratio, the production cross section of a Z boson and a jet from a b quark is remeasured in this analysis using exactly the same methodology as for the Z + c cross section. The remeasured Z + b cross section agrees with the published value within one standard deviation and is used in the ratio measurement.

The Z boson is identified through its decay into a pair of electrons or muons. Jets with HF quark content are identified through (1) the semileptonic decay of c or b flavoured hadrons with a muon in the final state, and (2) using exclusive hadronic decays of charm hadrons. The cross section and cross section ratio are measured at the level of stable particles, which are defined prior to the emission of any electroweak radiation. To minimize acceptance corrections, the measurements are restricted to a phase space that is close to the experimental fiducial volume with optimized sensitivity for the investigated processes: two leptons with transverse momentum $p_T^{\ell} > 20$ GeV, pseudorapidity $|\eta^{\ell}| < 2.1$, and dilepton invariant mass consistent with the mass of the Z boson, $71 < m_{\ell\ell} < 111$ GeV, together with a c (b) jet with $p_T^{\text{jet}} > 25$ GeV, $|\eta^{\text{jet}}| < 2.5$. The jet should be separated from the leptons of the Z boson candidate by a distance $\Delta R(\text{jet}, \ell) = \sqrt{(\Delta\eta)^2 + (\Delta\phi)^2} > 0.5$. The cross section $\sigma(\text{pp} \to \text{Z}+\text{c}+X)\mathcal{B}(\text{Z} \to \ell^+\ell^-)$ (abbreviated as $\sigma(\text{Z}+\text{c})\mathcal{B}$) and the cross section ratio $\sigma(\text{pp} \to \text{Z}+\text{c}+X)/\sigma(\text{pp} \to \text{Z}+\text{b}+X)$ (abbreviated as $\sigma(\text{Z}+\text{c})/\sigma(\text{Z}+\text{b})$) are determined both inclusively and differentially as a function of the transverse momentum of the Z boson, p_T^Z, and the p_T of the jet with heavy flavour content, p_T^{jet}.

The paper is structured as follows. The CMS detector is briefly described in Sect. 2, and the data and simulated samples used are presented in Sect. 3. Section 4 deals with the selection of the Z + HF jets signal sample, the auxiliary samples of events from the associated production of W+c, and top quark-antiquark (t$\bar{\text{t}}$) production. The determination of the c tagging efficiency is the subject of Sect. 5. The analysis strategy devised to separate the two contributions, Z+c and Z+b, in the sample of Z+HF jets is detailed in Sect. 6. Section 7 reviews the most important sources of systematic uncertainties and their impact on the measurements. Finally, the measurements of the inclusive Z+c cross section and the (Z+c)/(Z+b) cross section ratio are presented in Sect. 8, and the differential measurements are reported in Sect. 9. The main results of the paper are summarized in Sect. 10.

2 The CMS detector

The central feature of the CMS apparatus is a superconducting solenoid of 6 m internal diameter, providing a magnetic field of 3.8 T. Within the solenoid volume are a silicon pixel and strip tracker, a lead tungstate crystal electromagnetic calorimeter (ECAL), and a brass and scintillator hadron calorimeter, each composed of a barrel and two endcap sections. Extensive forward calorimetry complements the coverage provided by the barrel and endcap detectors. The silicon tracker measures charged particles within the pseudorapidity range $|\eta| < 2.5$. It consists of 1440 silicon pixel and 15 148 silicon strip detector modules. For nonisolated particles of $1 < p_T < 10$ GeV and $|\eta| < 1.4$, the track resolutions are typically 1.5% in p_T and 25–90 (45–150) μm in the transverse (longitudinal) impact parameter [18]. The electron momentum is estimated by combining the energy measurement in the ECAL with the momentum measurement in the tracker. The momentum resolution for electrons with $p_T \approx 45$ GeV from Z $\to$ e$^+$e$^-$ decays ranges from 1.7% for nonshowering electrons in the barrel region to 4.5% for showering electrons in the endcaps [19]. Muons are measured in the pseudorapidity range $|\eta| < 2.4$, using three technologies: drift tubes, cathode strip chambers, and resistive plate chambers. Matching muons to tracks measured in the silicon tracker results in a relative transverse momentum resolution for muons with $20 < p_T < 100$ GeV of 1.3–2.0% in the barrel and better than 6% in the endcaps. The p_T resolution in the barrel is better than 10% for muons with p_T up to 1 TeV [20]. For nonisolated muons with $1 < p_T < 25$ GeV, the relative transverse momentum resolution is 1.2–1.7% in the barrel and 2.5–4.0% in the endcaps [18]. The first level of the CMS trigger system [21], composed of custom hardware processors, uses information from the calorimeters and muon detectors to select events of interest in a fixed time interval of less than 4 μs. The high-level trigger processor farm further decreases the event rate from around 100 kHz to less than 1 kHz, before data storage. A more detailed description of the CMS detector, together with a definition of the coordinate system used and the basic kinematic variables, can be found in Ref. [22].

3 Data and simulated samples

The data were collected by the CMS experiment during 2012 at the pp centre-of-mass energy of 8 TeV and correspond to an integrated luminosity of $\mathcal{L} = 19.7 \pm 0.5$ fb^{-1}.

Samples of simulated events are produced with Monte Carlo (MC) event generators, both for the signal process and for the main backgrounds. A sample of signal Z boson events is generated with MADGRAPH v5.1.3.30 [23], interfaced with PYTHIA v6.4.26 [24] for parton showering and hadroniza-

tion using the MLM [25,26] matching scheme. The MAD-GRAPH generator produces parton-level events with a vector boson and up to four partons at leading order (LO) on the basis of a matrix-element calculation. The generation uses the parton distribution functions (PDF) set CTEQ6L [27]. The matching scale between jets from matrix element calculations and those produced via parton showers is 10 GeV, and the factorization and renormalization scales are set to $q^2 = M_Z^2 + (p_T^Z)^2$.

Other physics processes produce events with the same final state topology as the signal. The main background is the production of $t\bar{t}$ events. Smaller contributions are expected from the direct production of a pair of vector bosons: WW, WZ, and ZZ.

A sample of $t\bar{t}$ events is generated with POWHEG v1.0 [28–31], interfaced with PYTHIA6 and using the CT10 [32] PDF set. The WW, WZ, and ZZ processes are modelled with samples of events generated with PYTHIA6 and the CTEQ6L1 PDF set.

A sample of W boson events is generated with MAD-GRAPH interfaced with PYTHIA6. It is used in the determination of the c tagging efficiency and to validate the modelling of relevant distributions with a data sample of W+jets events. The matching scale between jets from matrix element calculations and those produced via parton showers is 10 GeV, and the factorization and renormalization scales are set to $q^2 = M_W^2 + (p_T^W)^2$. For all event generation the PYTHIA6 parameters for the underlying event modelling are set to the Z2* tune [33].

Generated events are processed through a full GEANT4-based [34] CMS detector simulation and trigger emulation. Simulated events are then reconstructed using the same algorithms as used to reconstruct collision data and are normalized to the integrated luminosity of the data sample using their respective cross sections. For electroweak processes the cross sections are evaluated to next-to-next-to-leading order (NNLO) with FEWZ 3.1 [35], using the MSTW2008NNLO [36] PDF set. The cross sections for diboson production are evaluated at next-to-leading order (NLO) with MCFM 6.6 [37] and using the MSTW2008NLO [36] PDF set. The $t\bar{t}$ cross section is taken at NNLO from Ref. [38]. The simulated samples incorporate additional pp interactions in the same or neighbouring bunch crossings (pileup). Simulated events are weighted so that the pileup distribution matches the measured one, with an average of about 21 pileup interactions per bunch crossing.

Simulated samples are corrected for differences between data and MC descriptions of lepton trigger, reconstruction, and selection efficiencies (ϵ_ℓ). Lepton efficiencies are evaluated with samples of dilepton events in the Z mass peak with the "tag-and-probe" method [39], and correction factors $\epsilon_\ell^{\text{data}}/\epsilon_\ell^{\text{MC}}$, binned in terms of p_T and η of the leptons,

are computed. These correction factors, based on the kinematics of each lepton in an event, are multiplied and used as an event weight.

The simulated signal sample includes Z boson events accompanied by jets originating from quarks of all flavours (b, c, and light). Events are classified as Z + b, Z + c, or Z + light flavour according to the flavour of the generator-level jets built from all showered particles after fragmentation and hadronization (all stable particles except neutrinos) and clustered with the same algorithm that is used to reconstruct data jets. A generator-level jet is defined to be b flavoured if $p_T^{\text{gen jet}} > 15$ GeV and there is a b hadron among the particles generated in the event within a cone of radius $\Delta R = 0.5$ around the jet axis. Similarly, a generator-level jet is considered to be c flavoured if $p_T^{\text{gen jet}} > 15$ GeV and there is a c hadron and no b hadrons within a cone of $\Delta R = 0.5$ around the jet axis. A Z + jets event is assigned as a Z + b event if there is at least a generator-level jet identified as a b flavoured jet regardless of the number of c flavoured or light jets, Z + c if there is at least a c flavoured jet at the generator-level and no b flavoured generator-level jets, and Z + light flavour otherwise.

4 Event reconstruction and selection

Electron and muon candidates are reconstructed following standard CMS procedures [19,20]. Jets, missing transverse energy, and related quantities are determined using the CMS particle-flow (PF) reconstruction algorithm [40], which identifies and reconstructs stable particle candidates arising from a collision with an optimized combination of the signals measured from all subdetectors.

Jets are built from PF candidates using the anti-k_T clustering algorithm [41] with a distance parameter of $R = 0.5$. The energy and momentum of the jets are corrected as a function of the jet p_T and η to account for the nonlinear response of the calorimeters and for the presence of pileup interactions [42,43]. Jet energy corrections are derived using samples of simulated events and further adjusted using dijet, photon+jet and Z+jet events in data.

The missing transverse momentum vector $\mathbf{p}_T^{\text{miss}}$ is the projection on the plane perpendicular to the beams of the negative vector sum of the momenta of all particles that are reconstructed with the PF algorithm. The missing transverse energy variable, E_T^{miss}, is defined as the magnitude of the $\mathbf{p}_T^{\text{miss}}$ vector, and it is a measure of the transverse energy of particles leaving the detector undetected [44].

The primary vertex of the event, representing the hard interaction, is selected among the reconstructed vertices as the one with the highest sum of the transverse momenta squared of the tracks associated to it.

4.1 Selection of Z + HF jet events

Events with a pair of leptons are selected online by a trigger system that requires the presence of two lepton candidates of the same flavour with $p_T > 17$ and 8 GeV for the leading-p_T and subleading-p_T lepton candidates, respectively. The analysis follows the offline selections as used in the CMS $Z \rightarrow e^+e^-$ and $Z \rightarrow \mu^+\mu^-$ inclusive analyses [39] and requires the presence of two high-p_T reconstructed leptons with opposite charges in the pseudorapidity region $|\eta^\ell| < 2.1$. The transverse momentum of the leptons has to be greater than 20 GeV.

The leptons are required to be isolated. The combined isolation I_{comb} is used to quantify the additional hadronic activity around the selected leptons. It is defined as the sum of the transverse energy of neutral hadrons and photons and the transverse momentum of charged particles in a cone with $R < 0.3$ (0.4) around the electron (muon) candidate, excluding the contribution from the lepton itself. Only charged particles originating from the primary vertex are considered in the sum to minimize the contribution from pileup interactions. The contribution of neutral particles from pileup vertices is estimated and subtracted from I_{comb}. For electrons, this contribution is evaluated with the jet area method described in Ref. [45]; for muons, it is taken to be half the sum of the p_T of all charged particles in the cone originating from pileup vertices. The factor one-half accounts for the expected ratio of charged to neutral particle energy in hadronic interactions. The electron (muon) candidate is considered to be isolated when $I_{comb}/p_T^\ell < 0.15$ (0.20). Finally, the analysis is restricted to events with a dilepton invariant mass, $m_{\ell\ell}$, in the range 91 ± 20 GeV in accordance with previous Z + jets measurements [17,46].

A Z + jets sample is selected by requiring the presence of at least one jet with $p_T^{jet} > 25$ GeV and $|\eta^{jet}| < 2.5$. Jets with an angular separation between the jet axis and any of the selected leptons less than $\Delta R(jet, \ell) = 0.5$ are not considered. To reduce the contribution from $t\bar{t}$ events, we require E_T^{miss} to be smaller than 40 GeV.

Hadrons with c or b quark content decay weakly with lifetimes of the order of 10^{-12} s and mean decay lengths larger than $100\,\mu$m at the LHC energies. Secondary vertices well separated from the primary vertex can be reconstructed from the tracks of their charged decay products. We focus on the following three signatures to identify jets originating from a heavy flavour quark:

- **Semileptonic mode** – A semileptonic decay of a heavy flavour hadron leading to a well-identified muon associated to a displaced secondary vertex.
- **D$^\pm$ mode** – A displaced secondary vertex with three tracks consistent with a $D^\pm \rightarrow K^\mp \pi^\pm \pi^\pm$ decay.

- **D*(2010)$^\pm$ mode** – A displaced secondary vertex with two tracks consistent with a $D^0 \rightarrow K^-\pi^+$ ($\overline{D}^0 \rightarrow K^+\pi^-$) decay and associated with a $D^{*+}(2010) \rightarrow D^0\pi^+$ ($D^{*-}(2010) \rightarrow \overline{D}^0\pi^-$) decay at the primary vertex.

Displaced secondary vertices for the first two categories are formed with either the Simple Secondary Vertex (SSV) [47] or the Inclusive Vertex Finder (IVF) [48,49] CMS vertex reconstruction algorithms. Both algorithms follow the adaptive vertex fitter technique [50] to construct a secondary vertex, but differ in the tracks used. The SSV algorithm takes as input the tracks constituting the jet; the IVF algorithm starts from a displaced track with respect to the primary vertex (*seed* track) and searches for nearby tracks, in terms of their separation distance in three dimensions and their angular separation around this *seed*, to build the vertex. Tracks used in a secondary vertex reconstruction must have $p_T > 1$ GeV. Vertices reconstructed with the IVF algorithm are considered first because of the higher efficiency of the algorithm. If no IVF vertex is found, SSV vertices are searched for, thus providing additional event candidates. We employ a different technique for the third (D*(2010)$^\pm$ mode) category, as described below in the text. The typical mass resolution in the D$^\pm$ and D*(2010)$^\pm$ reconstruction is ≈ 17 MeV in the decay modes analyzed here.

4.1.1 Selection in the semileptonic mode

The Z+c (Z+b) events with a semileptonic c (b) quark decay are selected by looking for a reconstructed muon (*muon-inside-a-jet*) among the constituents of any of the selected jets. This *muon-inside-a-jet* candidate has to satisfy the same quality criteria as those imposed on the muons from the Z boson decay. The muon has to be reconstructed in the region $|\eta^\mu| < 2.4$, with $p_T^\mu < 25$ GeV, $p_T^\mu/p_T^{jet} < 0.6$, and it should not be isolated from hadron activity. The combined isolation has to be large, $I_{comb}/p_T^\mu > 0.2$. Furthermore, the *muon-inside-a-jet* is required to be associated to a secondary vertex, reconstructed either with the IVF or SSV algorithm. No minimum p_T is required for the muon beyond the general $p_T > 1$ GeV requirement for the tracks used in the reconstruction of the secondary vertices. Muon reconstruction sets a natural threshold of $p_T \gtrsim 3$ GeV in the barrel region and $p_T \gtrsim 2$ GeV in the endcaps to ensure the muon passes the material in front of the muon detector and travels deep enough into the muon system to be reconstructed and satisfy the identification criteria [39]. The above selection results in 4145 events in the $Z \rightarrow e^+e^-$ channel and 5258 events in the $Z \rightarrow \mu^+\mu^-$ channel.

Figure 1 shows the transverse momentum distribution of the selected *muon-inside-a-jet* for $Z \rightarrow e^+e^-$ (left) and $Z \rightarrow$
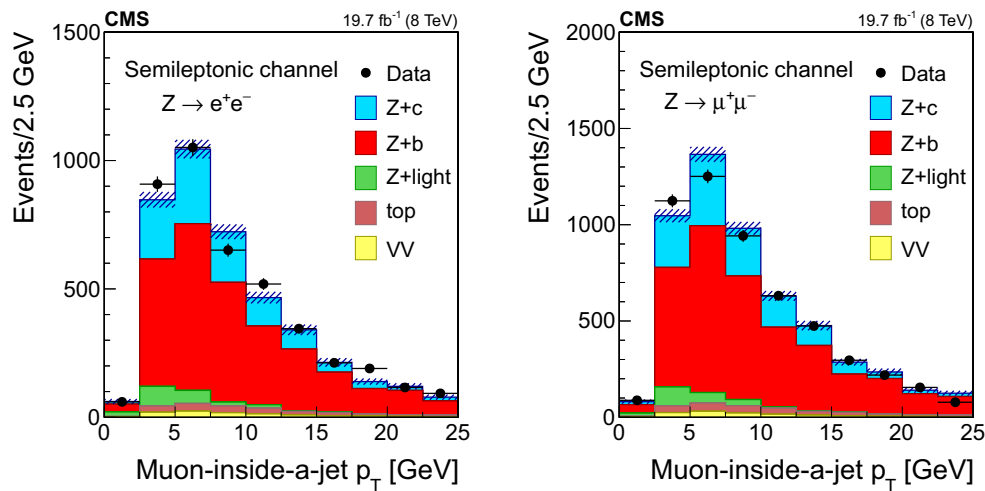
Fig. 1 Transverse momentum distribution of the selected *muon-inside-a-jet* for events with an identified muon among the jet constituents, in the dielectron (left) and dimuon (right) channels. The contributions from all processes are estimated with the simulated samples. Vertical bars on data points represent the statistical uncertainty in the data. The hatched areas represent the statistical uncertainty in the MC simulation

$\mu^+\mu^-$ (right). The data are compared with the predictions of the MC simulations, which are composed of Z+b events ($\approx 65\%$), Z+c events ($\approx 25\%$), Z+light flavour ($\lesssim 5\%$), and other backgrounds, such as $t\bar{t}$ and diboson production ($\approx 5\%$).

4.1.2 Selection in the $D^\pm$ mode

Event candidates in the $D^\pm$ mode are selected by looking for secondary vertices made of three tracks and with a reconstructed invariant mass consistent with the $D^\pm$ mass: 1869.5 ± 0.4 MeV [51]. The sum of the charges of the tracks participating in the secondary vertex must be ± 1. The kaon mass is assigned to the track with opposite sign to the total charge of the three-prong vertex, and the remaining tracks are assumed to have the mass of a charged pion. This assignment is correct in more than 99% of the cases, since the fraction of double Cabibbo-suppressed decays is extremely small [51].

The distribution of the reconstructed invariant mass for $D^\pm$ candidates associated with $Z \rightarrow e^+e^-$ (left) and $Z \rightarrow \mu^+\mu^-$ (right) is presented in Fig. 2. The signal and background contributions shown in the figure are estimated with the simulated samples. The charm fraction $\mathcal{B}(c \rightarrow D^\pm)$ in the PYTHIA simulation $(19.44 \pm 0.02)\%$ is lower than the value $(22.7 \pm 0.9 \pm 0.5)\%$ obtained from a combination [52] of published measurements performed at LEP [53–55] and the branching fraction of the decay $D^\pm \rightarrow K^\mp\pi^\pm\pi^\pm$ $(7.96 \pm 0.03)\%$, is also lower than the PDG value $(9.13 \pm 0.19)\%$ [51]; predicted event rates from the MC simulation are scaled in order to match the experimental charm fractions.

The signal region is defined by the constraint $\Delta m(D^\pm) \equiv |m^{\mathrm{rec}}(D^\pm) - 1.87\,\mathrm{GeV}| < 0.05\,\mathrm{GeV}$, where $m^{\mathrm{rec}}(D^\pm)$ is the reconstructed mass of the $D^\pm$ meson candidate. The

mass range of the signal region is indicated in Fig. 2 as two dashed, vertical lines. The width of the signal region approximately corresponds to three times the measured mass resolution. The nonresonant background is subtracted from the event count in the signal window, and is estimated using the number of events selected in a control region away from the resonance, extending up to a window of 0.1 GeV width, $N[0.05 < \Delta m(D^\pm) < 0.10\,\mathrm{GeV}]$, as also shown in Fig. 2.

The number of selected events in data after background subtraction is 375 ± 44 in the $Z \rightarrow e^+e^-$ channel and 490 ± 48 in the $Z \rightarrow \mu^+\mu^-$ channel. Based on the simulation, the selected sample is enriched in Z+c events ($\approx 60\%$), while the fraction of Z+b events is $\approx 35\%$. The contribution from Z+light flavour events is negligible, and the contribution of $t\bar{t}$ and diboson events is smaller than 5%.

4.1.3 Selection in the $D^*(2010)^\pm$ mode

Events with Z+jets candidates in the $D^*(2010)^\pm$ mode are selected by requiring a displaced vertex with two oppositely charged tracks among the tracks constituting the jet. These tracks are assumed to be the decay products of a D^0 meson. The candidate is combined with a third track from the jet constituents that should represent the *soft pion*, emitted in the strong decay $D^{*+}(2010) \rightarrow D^0\pi^+$. To be a *soft pion* candidate, the track must have a transverse momentum larger than 0.5 GeV and lie in a cone of radius $\Delta R(D^0, \pi) = 0.1$ around the line of flight of the D^0 meson candidate.

The track of the D^0 meson candidate with a charge opposite to the charge of the *soft pion* is taken to be the kaon from the D^0 meson decay and is required to have $p_T > 1.75$ GeV. The other track is assigned to be the pion and is required
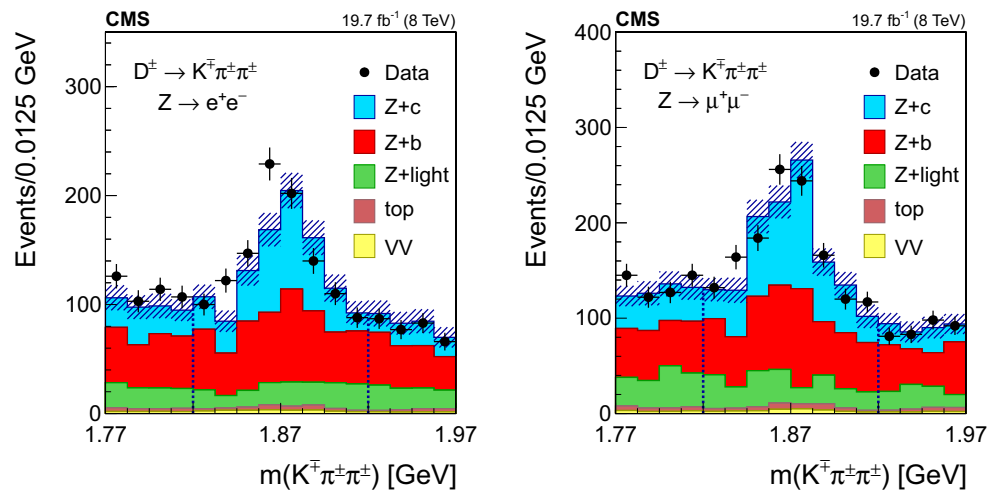
Fig. 2 The invariant mass distribution of three-prong secondary vertices for events selected in the $D^\pm$ mode, in the dielectron (left) and dimuon (right) channels. The mass assigned to each of the three tracks is explained in the text. The contributions from all processes are estimated with the simulated samples. The two dashed, vertical lines indicate the mass range of the signal region. Vertical bars on data points represent the statistical uncertainty in the data. The hatched areas represent the statistical uncertainty in the MC simulation

to have $p_T > 0.75$ GeV. Two-track combinations with an invariant mass different from the nominal D^0 meson mass (1864.86 ± 0.13 MeV) by less than 100 MeV are selected, and a secondary vertex is constructed using the two tracks and the CMS Kalman vertex fitter algorithm [56]. The two-track system is kept as a valid D^0 meson candidate if the probability for the vertex fit is greater than 0.05.

To ensure a clean separation between the secondary and primary vertices, the 2D-distance in the transverse plane between them, divided by the uncertainty in the distance measurement (defined as decay length significance) has to be larger than 3. Furthermore, to guarantee that the reconstructed vertex corresponds to a two-body decay of a hadron originating at the primary vertex, the momentum vector of the D^0 meson candidate has to be collinear with the line from the primary vertex to the secondary vertex: the cosine of the angle between the two directions has to be larger than 0.99. Finally, only events with a mass difference between the $D^*(2010)^\pm$ and D^0 candidates within 5 MeV from the expected value (145.426 ± 0.002 MeV [51]) are selected.

The product of the branching fractions $\mathcal{B}(c \rightarrow D^{*+}(2010))\mathcal{B}(D^{*+}(2010) \rightarrow D^0\pi^+)\mathcal{B}(D^0 \rightarrow K^-\pi^+)$ (+ charge conjugate) in the PYTHIA simulation is $(0.741 \pm 0.005)\%$, which is about 15% larger than the average of the experimental values, $(0.622 \pm 0.020)\%$ [51,52]. Therefore, expected event rates from the MC simulation are scaled in order to match the experimental values.

The distribution of the reconstructed mass of the $D^*(2010)^\pm$ candidates is presented in Fig. 3 for events with a Z boson decaying into e^+e^- (left) and $\mu^+\mu^-$ (right). The contribution from the different processes is estimated with the simulated samples.

The signal region is defined by the constraint $\Delta m(D^*(2010)^\pm) \equiv |m^{rec}(D^*(2010)^\pm) - 2.01 \text{ GeV}| < 0.04$ GeV, where $m^{rec}(D^*(2010)^\pm)$ is the reconstructed mass of the $D^*(2010)^\pm$ candidate, and which corresponds to slightly more than twice the measured mass resolution. The two dashed, vertical lines present in Fig. 3 indicate the mass range of the signal region. The nonresonant background contribution to the signal region is subtracted using the number of events selected in a control region away from the resonance. We use a window of 0.12 (2×0.06) GeV width, $N[0.04 < \Delta m(D^*(2010)^\pm) < 0.10 \text{ GeV}]$, also shown in Fig. 3, and apply the proper weight to account for the different width of the signal and control regions (8/12).

The number of data selected events after background subtraction is 234 ± 22 in the $Z \rightarrow e^+e^-$ channel and 308 ± 24 in the $Z \rightarrow \mu^+\mu^-$ channel. According to the predictions obtained from the simulated samples, the fraction of $Z + c$ events in the selected sample is high ($\approx 65\%$) and the contribution of $Z+b$ events is $\approx 30\%$. No contribution is expected from $Z +$ light flavour events. Less than 5% of the selected events arise from $t\bar{t}$ and diboson production.

Systematic biases due to the background subtraction are expected to be negligible compared to the statistical uncertainty, because of the approximate agreement observed between data and simulation as shown in Figs. 2 and 3.

4.2 Selection of W+charm jet events (c jet control sample)

Additional data and simulated samples consist of events from associated production of a W boson and a jet originating from a c quark (W + c). They are used to model characteristic distributions of jets with c quark content and to measure the c
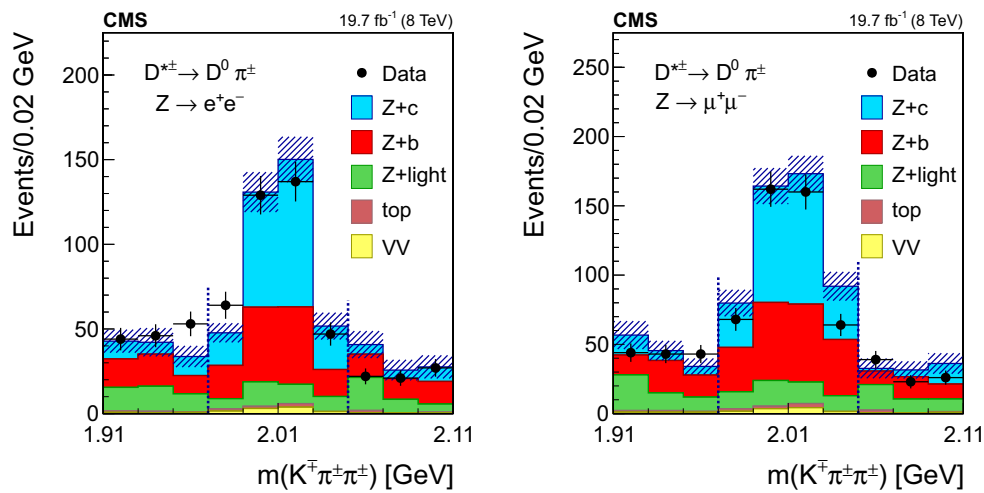
Fig. 3 The invariant mass distribution of the three-track system composed of a two-prong secondary vertex and a primary particle for events selected in the D*(2010)$^{\pm}$ mode, in the dielectron (left) and dimuon (right) channels. The mass assigned to each of the three tracks is explained in the text. The contributions from all processes are esti-mated with the simulated samples. The two dashed, vertical lines mark the mass range of the signal region. Vertical bars on data points represent the statistical uncertainty in the data. The hatched areas represent the statistical uncertainty in the MC simulation

tagging efficiency in a large, independent sample. Jet flavour assignment in the simulated W + jets events follows the criteria presented in Sect. 3 for Z + jets events.

The production of a W boson in association with a c quark proceeds at LO via the processes $qg \rightarrow W^- + c$ and $\bar{q}g \rightarrow W^{\mp}$ (q = s, d). A key property of the $qg \rightarrow W + c$ reaction is the presence of a charm quark and a W boson with opposite-sign (OS) charges. Background processes deliver OS and same-sign (SS) events in equal proportions, whereas $qg \rightarrow W + c$ is always OS. Therefore, distributions obtained after OS − SS subtraction are representative of the W + c component, allowing for detailed studies of c jets.

We select W+c events following the criteria of the analysis reported in Ref. [57]. Candidate events are selected online using single-lepton triggers, which require at least one isolated electron (muon) with $p_T > 27$ (24) GeV and $|\eta^{\ell}| < 2.1$. The lepton identification and isolation criteria are very similar to those used for the Z+jets selection. The offline p_T threshold is increased to 30 (25) GeV for electrons (muons) because of the higher thresholds of the single-lepton triggers. The transverse invariant mass of the lepton and $\mathbf{p}_T^{\text{miss}}$ system is defined as $M_T = \sqrt{2\, p_T^{\ell}\, E_T^{\text{miss}} [1 - \cos(\phi^{\ell} - \phi^{E_T^{\text{miss}}})]}$, where ϕ^{ℓ} and $\phi^{E_T^{\text{miss}}}$ are the azimuthal angles of the lepton momentum and $\mathbf{p}_T^{\text{miss}}$. The M_T must be larger than 55 (50) GeV for events in the $W \rightarrow e\nu$ ($W \rightarrow \mu\nu$) channel.

Identification of jets originating from c quarks proceeds exactly as described in Sect. 4.1. In all cases the charge of the c quark is unequivocally known. In the semileptonic mode the charge of the muon determines the charge of the c quark. In

the D$^{\pm}$ and D*(2010)$^{\pm}$ modes the charge of the D candidates defines the charge of the c quark. OS events are events when the muon, D$^{\pm}$, or D*(2010)$^{\pm}$ candidate has a charge opposite to the lepton from the W boson decay, and SS events when the charge is the same.

Based on the simulations, after subtracting the SS from the OS samples, W + c events are the dominant contributor to the distributions; ≈ 90% in the semileptonic decay modes and larger than 98% in the D$^{\pm}$ and D*(2010)$^{\pm}$ exclusive channels. The remaining backgrounds, mainly from top quark production, are subtracted using the simulation.

4.3 Selection of t̄t samples

A sample of t̄t events (eμ-t̄t sample) is selected using the leptonic decay modes of the W bosons from the t̄t pair when they decay into leptons of different flavour. The t̄t production is a natural source of b flavoured jets and enables tests of the MC description of the relevant distributions for b jets as well as of the performance of the secondary vertexing method. This sample is also used to model the t̄t background in the discriminant variables used to extract the signal yields.

An eμ-t̄t sample is selected online by a trigger path based on the presence of an electron-muon pair. The offline selection proceeds as for the Z+HF jet events, but the two leptons must be different flavours. After the selection, contributions from processes other than t̄t production are negligible.

An additional t̄t enriched sample is used to estimate the normalization of the remaining t̄t background. The same selection used for the Z+HF jet signal is applied: two leptons of the same flavour, ee or μμ, and $E_T^{\text{miss}} > 80$ GeV, instead

of $E_T^{miss} < 40$ GeV. The small contribution from $Z + jets$ events in these samples ($\lesssim 3\%$) is subtracted according to its MC expectation.

5 Measurement of the c and b quark tagging efficiencies

The accuracy of the description in the MC simulations of the secondary vertex reconstruction part of the c tagging method is evaluated with a control sample of $W + c$ events with a well-identified *muon-inside-a-jet*. The events are selected as described in Sect. 4.2 except for the requirement that the *muon-inside-a-jet* must come from a secondary vertex. The $OS - SS$ strategy suppresses all backgrounds to the $W + c$ sample in the $W \to \mu\nu$ decay mode except for Drell–Yan events. The contamination from the Drell–Yan process, which yields genuine OS dimuon events may reach 25%. The $W + c$ sample in the $W \to e\nu$ decay mode, with the lepton from the W decay of different flavour from the *muon-inside-a-jet*, is not affected by this background and is employed for the c tagging study.

A $W + c$ event is "SV-tagged" if there is a reconstructed secondary vertex in the jet and the *muon-inside-a-jet* is one of the tracks used to form the vertex. The c jet tagging efficiency is the fraction of "SV-tagged" $W + c$ events, over all $W + c$ events, after $OS - SS$ subtraction:

$$\epsilon_c = \frac{N(W+c)^{OS-SS}(SV\text{-tagged})}{N(W+c)^{OS-SS}}.$$

Efficiencies are obtained independently with the data and with the W+jets simulated samples. Data-to-simulation scale factors, SF_c, are then computed as the ratio between the c jet tagging efficiencies in data and simulation,

$$SF_c = \frac{\epsilon_c^{data}}{\epsilon_c^{MC}}.$$

They are used to correct the simulation efficiency.

The c jet tagging efficiencies and the scale factors are computed both inclusively and as a function of the jet p_T. The expected average c tagging efficiency is $\approx 33\%$ for the IVF algorithm and $\approx 21\%$ for the SSV algorithm. The c tagging efficiency ranges from 24% for the IVF algorithm (15% for the SSV algorithm) for p_T^{jets} of 25–30 GeV and up to 37% (26%) for p_T^{jets} of ≈ 100 GeV. The SF_c for jets with a p_T larger than 25 GeV is found to be 0.93 ± 0.03 (stat) ± 0.02 (syst) for IVF vertices. It is 0.92 ± 0.03 (stat) ± 0.02 (syst) for SSV vertices. The systematic uncertainty accounts for inaccuracies in pileup description, jet energy scale and resolution, lepton efficiencies, background subtraction, and modelling of charm production and decay fractions in the simulation.

Detailed studies of the behaviour of the b tagging methods developed in CMS are available in Ref. [58]. Following the same procedure, we have used the $e\mu$-$t\bar{t}$ sample to investigate the data-to-MC agreement for the b tagging methods in this analysis. The b tagging efficiencies in data and simulated events are computed as the fraction of $e\mu$-$t\bar{t}$ events with a *muon-inside-a-jet* participating in a secondary vertex with respect to the number of events when the secondary vertex condition is released. The $SF_b = \epsilon_b^{data}/\epsilon_b^{MC}$ is measured to be 0.96 ± 0.03 for both IVF and SSV vertices, where the uncertainty includes statistical and systematic effects due to the jet energy scale and resolution and the pileup.

6 Analysis strategy

The extraction of $Z + c$ and $Z + b$ event yields is based on template fits to distributions of variables sensitive to the jet flavour. In the semileptonic mode we use the corrected invariant mass, M_{vertex}^{corr} (corrected secondary-vertex mass), of the charged particles attached to the secondary vertex (the *muon-inside-a-jet* included). All charged particles are assigned the mass of the pion, except for the identified muon. A correction is included to account for additional particles, either charged or neutral, that may have been produced in the semileptonic decay but were not reconstructed [59],

$$M_{vertex}^{corr} = \sqrt{M_{vertex}^2 + p_{vertex}^2 \sin^2\theta} + p_{vertex}\sin\theta,$$

where M_{vertex} and p_{vertex} are the invariant mass and modulus of the vectorial sum of the momenta of all reconstructed particles associated to the secondary vertex, and θ is the angle between the momentum vector sum and the vector from the primary to the secondary vertex.

In the $D^{\pm}$ and $D^*(2010)^{\pm}$ modes a likelihood estimate of the probability that the jet tracks come from the primary vertex, called jet probability (JP) discriminant [47], is used.

The shapes of the Z+c discriminant distributions are modelled in data using OS $W + c$ events, after subtraction of the SS $W + c$ distributions. It is checked using simulated events that the corresponding distributions obtained from the $W + c$ samples accurately describe the Z+c distributions. The main features of the jets, such as p_T, η, jet charged multiplicity, and the number of secondary vertices are found to be consistent between $Z + c$ and $W + c$ simulated samples and are in agreement with the observed distributions in the sample of $W + c$ events in data. Figure 4 (left) shows the simulated p_T^{jet} distributions of $W + c$ and $Z + c$ events compared to $W + c$ data after $OS - SS$ subtraction. The number of secondary vertices, identified with the IVF algorithm, is shown in Fig. 4 (right). Events with no reconstructed IVF vertices
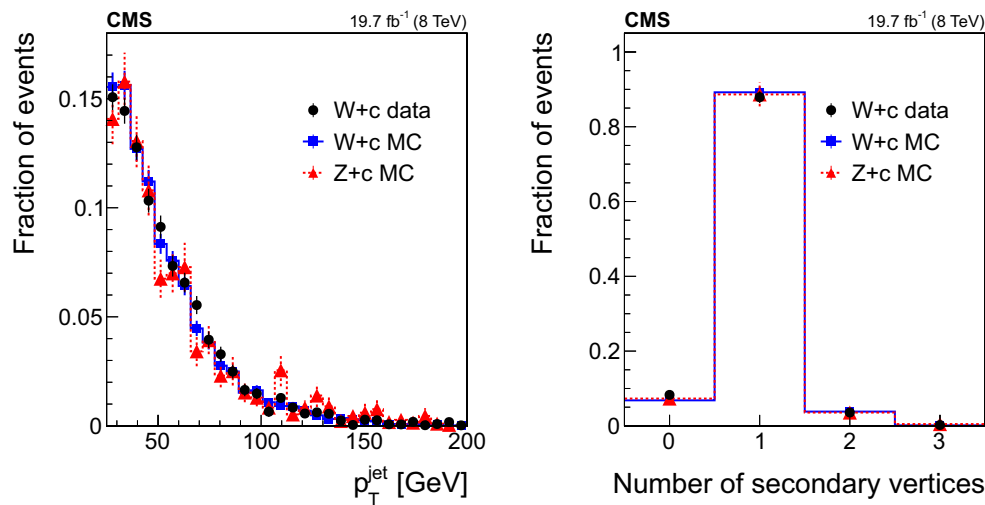
Fig. 4 Transverse momentum distribution of the c-tagged jet (left) and number of reconstructed secondary vertices (right), normalized to unity, in simulated W + c and Z + c samples and in W + 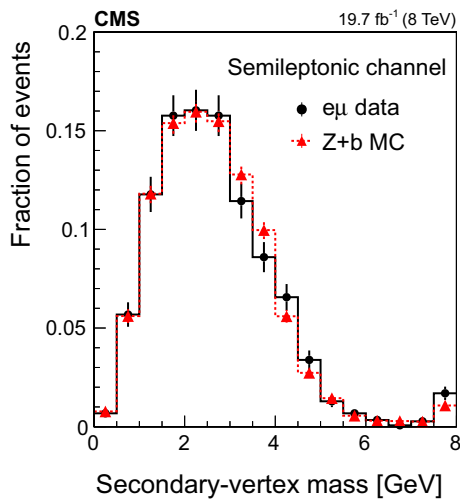c data events. The W+c distributions are presented after the OS−SS subtraction. Vertical bars represent the statistical uncertainties
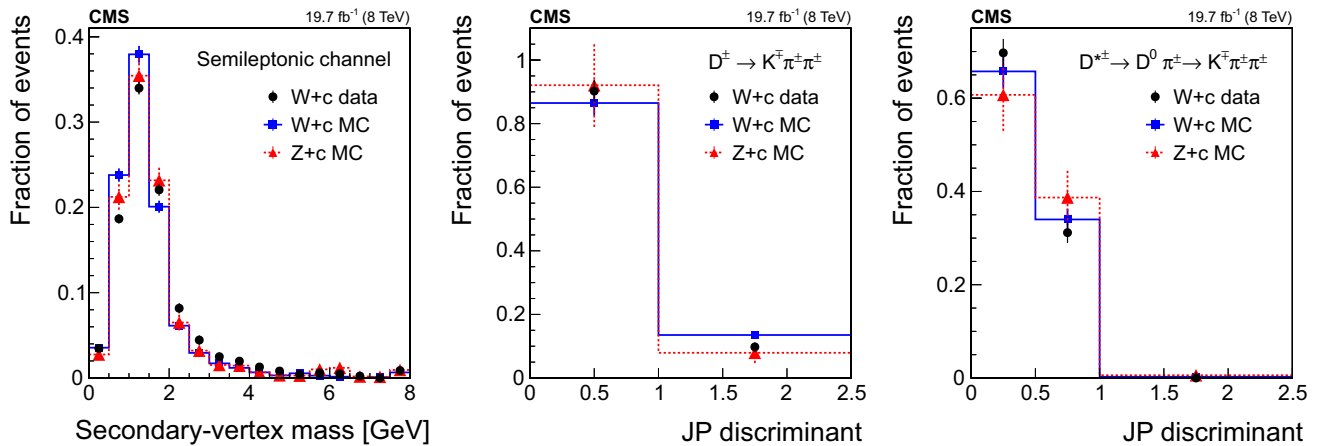
Fig. 5 Distributions of the corrected secondary-vertex mass (left plot) and JP discriminant (D$^{\pm}$ and D*(2010)$^{\pm}$ modes in the middle and right plots), normalized to unity, in simulated W + c and Z + c samples, and in W + c data events. The W + c distributions are presented after the OS − SS subtraction. Events with $M_{\mathrm{vertex}}^{\mathrm{corr}} > 8$ GeV are included in the last bin of the corrected secondary-vertex mass distribution. Vertical bars represent the statistical uncertainties

have at least one reconstructed vertex with the SSV vertex algorithm. All distributions in Fig. 4 are normalized to unity.

The corrected secondary-vertex mass and JP discriminant distributions, normalized to unity, are presented in Fig. 5 for the three analysis categories. The simulated W + c and Z + c distributions are compared to W + c data. In general, the simulated W + c and Z + c distributions agree with the W + c data in all categories. A noticeable discrepancy is observed between the simulated and measured distributions of the corrected secondary-vertex mass in W + c events as shown in Fig. 5 (left). This difference is due to a different fraction of events with two- and three-track vertices in data and in the simulation. Studies with simulated events demonstrate that

the fraction of events with two- and three-track vertices for W+c and Z+c production is the same. Therefore, we assume that the W + c corrected secondary-vertex mass distribution measured in data properly reproduces the same distribution for the Z + c measured events. The distributions obtained in the electron and muon decay channels are consistent and are averaged to obtain the final templates, thereby decreasing the associated statistical uncertainty.

The shape of the discriminant variables for Z+b events is modelled with the simulated samples. The simulated distribution of the corrected secondary-vertex mass is validated with the sample of eμ-t$\bar{\mathrm{t}}$ events as shown in Fig. 6. The simulation describes the data well, apart from the mass regions 3–4 GeV

Fig. 6 Distribution of the corrected secondary-vertex mass normalized to unity from simulated Z+b and eμ-tt̄ data (described in the text) events. Vertical bars represent the statistical uncertainties. The last bin of the distribution includes events with $M_{vertex}^{corr} > 8$ GeV

and above 7.5 GeV. The observed differences, $\approx 13\%$ in the 3–4 GeV mass region and $\approx 50\%$ above 7.5 GeV, are used to correct the simulated Z+b distribution. However, the number of events in the eμ-tt̄ sample does not allow a validation of the shape of JP discriminant distributions for Z+b events in the exclusive channels.

The distributions of the discriminant variables obtained in data are corrected by subtracting the contributions from the various background processes. They are estimated in the following way:

- The shapes of the discriminant distributions for tt̄ production are evaluated with the eμ-tt̄ sample. The normalization difference between same and different flavour combinations, $N_{ee}^{tt̄}/N_{eμ}^{tt̄}$ ($N_{μμ}^{tt̄}/N_{eμ}^{tt̄}$) is estimated from the sideband region $E_T^{miss} > 80$ GeV, and applied to the signal region $E_T^{miss} < 40$ GeV.
- The shape and normalization of the corrected secondary-vertex mass distribution for the Z + light flavour quark background in the semileptonic channel are evaluated with the simulated samples. Discrepancies between data and simulation in the rate of Z+light flavour jet misidentification are corrected by applying the appropriate scale factors to the simulation [58]. No background from the Z+light flavour quark process is expected in the exclusive channels.
- The shapes and normalization of the discriminant distributions for the remaining background from diboson production are taken from simulation.

The yields of Z+c and Z+b events in data are estimated by performing least squares fits between the background-

subtracted data and template distributions. Independent fits are performed in the dielectron and dimuon channels and in the three analysis categories. The expected Z+c and Z+b distributions are fitted to data with scaling factors μ_{Z+c} and μ_{Z+b} defined with respect to the initial normalization predicted from simulation as free parameters of the fit. Typical values of the scaling factors are in the range 0.95–1.05 with a correlation coefficient between μ_{Z+c} and μ_{Z+b} of the order of -0.4. The scaling factor obtained for the Z + b component is consistent with that reported in Ref. [17] for a similar fiducial region. The fitted μ_{Z+c} and μ_{Z+b} are applied to the expected yields to obtain the measured ones in the data. The measured yields are summarized in Table 1.

Figure 7 shows the background-subtracted distributions of the corrected secondary-vertex mass for the Z + jets events with a *muon-inside-a-jet* associated with a secondary vertex. The corrected secondary-vertex mass tends to be larger for Z + b than for Z + c events because the larger mass of the b quark gives rise to heavier hadrons ($m_{b\,hadrons} \approx 5$ GeV, $m_{c\,hadrons} \approx 2$ GeV).

The JP discriminant takes lower values for Z + c events than for Z+b events. The $D^{\pm}$ or $D^*(2010)^{\pm}$ mesons in Z+b events are "secondary" particles, i.e. they do not originate from the hadronization of a c quark produced at the primary vertex, but are decay products of previous b hadron decays at unobserved secondary vertices. Figure 8 shows the background-subtracted distribution of the JP discriminant for the Z + jets events with a $D^{\pm} \rightarrow K^{\mp}\pi^{\pm}\pi^{\pm}$ candidate. Two bins are used to model the JP discriminant in this channel; as a result, the determination of the scaling factors μ_{Z+c} and μ_{Z+b} is reduced to solving a system of two equations with two unknowns.

Figure 9 presents the background-subtracted distribution of the JP discriminant for the Z+jets events with a $D^*(2010)^{\pm}$ candidate. In this latter channel the particle identified as the *soft pion* in the $D^*(2010)^{\pm} \rightarrow D^0\pi^{\pm}$ decay is a true primary particle in the case of Z+c events, whereas it arises from a secondary decay (b hadron $\rightarrow D^*(2010)^{\pm} + X \rightarrow D^0\pi^{\pm} + X$) for Z+b events. This "secondary" origin of the *soft pion* generates a distinctive dip in the first bin of the JP discriminant distribution for Z+b events.

7 Systematic uncertainties

Several sources of systematic uncertainties are identified, and their impact on the measurements is estimated by performing the signal extraction fit with the relevant parameters in the simulation varied up and down by their uncertainties. The effects are summarized in Fig. 10. The contributions from the various sources are combined into fewer categories for presentation in Fig. 10.

Table 1 Cross section $\sigma(Z+c)\,\mathcal{B}$ and cross section ratio $\sigma(Z+c)/\sigma(Z+b)$ in the three categories of this analysis and in the two Z boson decay channels. The N_{Z+c}^{signal} and N_{Z+b}^{signal} are the yields of Z+c and Z+b events, respectively, extracted from the fit to the corrected secondary-vertex mass (semileptonic mode) or JP discriminant ($D^{\pm}$ and $D^*(2010)^{\pm}$ modes) distributions. The factors $\mathcal{C}$ that correct the selection inefficiencies are also given. They include the relevant branching fraction for the corresponding channel. All uncertainties quoted in the table are statistical, except for those of the measured cross sections and cross section ratios where the first uncertainty is statistical and the second is the estimated systematic uncertainty from the sources discussed in the text

Channel	N_{Z+c}^{signal}	$\mathcal{C}_{Z+c}$ (%)	$\sigma(Z+c)\,\mathcal{B}$ [pb]
Semileptonic mode			
$Z \to e^+e^-$	1070 ± 100	0.63 ± 0.03	$8.6 \pm 0.8 \pm 1.0$
$Z \to \mu^+\mu^-$	1450 ± 140	0.81 ± 0.03	$9.1 \pm 0.9 \pm 1.0$
$Z \to \ell^+\ell^-$	$\sigma(Z+c)\,\mathcal{B} = 8.8 \pm 0.6\,\text{(stat)} \pm 1.0\,\text{(syst)}$ pb		

Channel	N_{Z+b}^{signal}	$\mathcal{C}_{Z+b}$ (%)	$\sigma(Z+c)/\sigma(Z+b)$
$Z \to e^+e^-$	2610 ± 110	2.90 ± 0.08	$1.9 \pm 0.2 \pm 0.2$
$Z \to \mu^+\mu^-$	3240 ± 150	3.93 ± 0.10	$2.2 \pm 0.3 \pm 0.2$
$Z \to \ell^+\ell^-$	$\sigma(Z+c)/\sigma(Z+b) = 2.0 \pm 0.2\,\text{(stat)} \pm 0.2\,\text{(syst)}$		

Channel	N_{Z+c}^{signal}	$\mathcal{C}_{Z+c}$ (%)	$\sigma(Z+c)\,\mathcal{B}$ [pb]
$D^{\pm}$ mode			
$Z \to e^+e^-$	280 ± 60	0.13 ± 0.02	$10.9 \pm 2.2 \pm 0.9$
$Z \to \mu^+\mu^-$	320 ± 80	0.18 ± 0.02	$8.8 \pm 2.0 \pm 0.8$
$Z \to \ell^+\ell^-$	$\sigma(Z+c)\,\mathcal{B} = 9.7 \pm 1.5\,\text{(stat)} \pm 0.8\,\text{(syst)}$ pb		

| Channel	N_{Z+c}^{signal}	$\mathcal{C}_{Z+c}$ (%)	$\sigma(Z+c)\,\mathcal{B}$ [pb]
$D^*(2010)^{\pm}$ mode			
$Z \to e^+e^-$	150 ± 30	0.11 ± 0.01	$7.3 \pm 1.5 \pm 0.5$
$Z \to \mu^+\mu^-$	250 ± 30	0.14 ± 0.01	$9.3 \pm 1.1 \pm 0.7$
$Z \to \ell^+\ell^-$	$\sigma(Z+c)\,\mathcal{B} = 8.5 \pm 0.9\,\text{(stat)} \pm 0.6\,\text{(syst)}$ pb		
Combination			
$Z \to \ell^+\ell^-$	$\sigma(Z+c)\,\mathcal{B} = 8.8 \pm 0.5\,\text{(stat)} \pm 0.6\,\text{(syst)}$ pb		
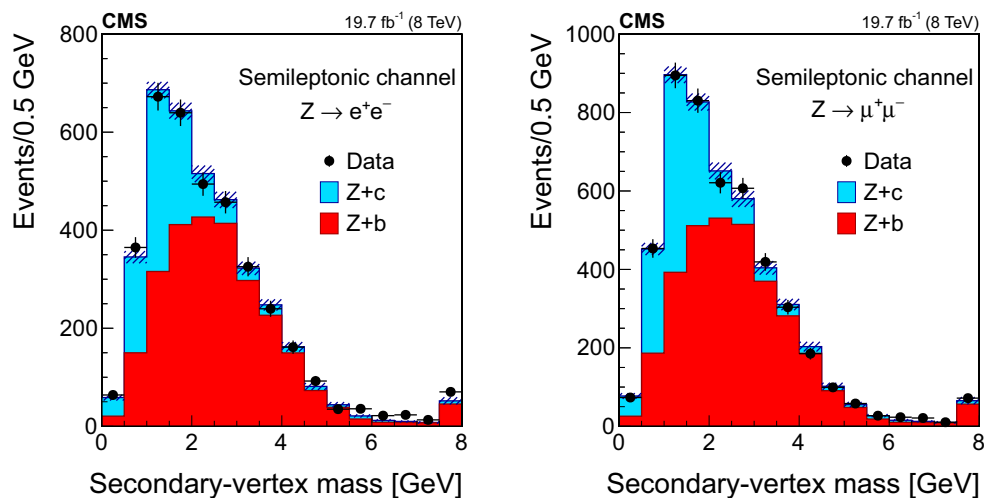
Fig. 7 Corrected secondary-vertex mass distributions, after background subtraction, in the dielectron (left) and dimuon (right) channels for events selected in the semileptonic mode. Events with $M_{\text{vertex}}^{\text{corr}} > 8$ GeV are included in the last bin of the distribution. The shape of the Z + c and Z + b contributions is estimated as explained in the text. Their normalization is adjusted to the result of the signal extraction fit. Vertical bars on data points represent the statistical uncertainty in the data. The hatched areas represent the sum in quadrature of the statistical uncertainties of the templates describing the two contributions (Z + c from W + c data events and Z + b from simulation)

One of the main uncertainties is related to the charm fractions for the production and decay of c hadrons in the simulated samples and to the determination of the c tagging efficiency. The average of the inclusive charm quark semileptonic branching fractions is $\mathcal{B}(c \to \ell) = 0.096 \pm 0.004$ [51], and the exclusive sum of the individual contributions from
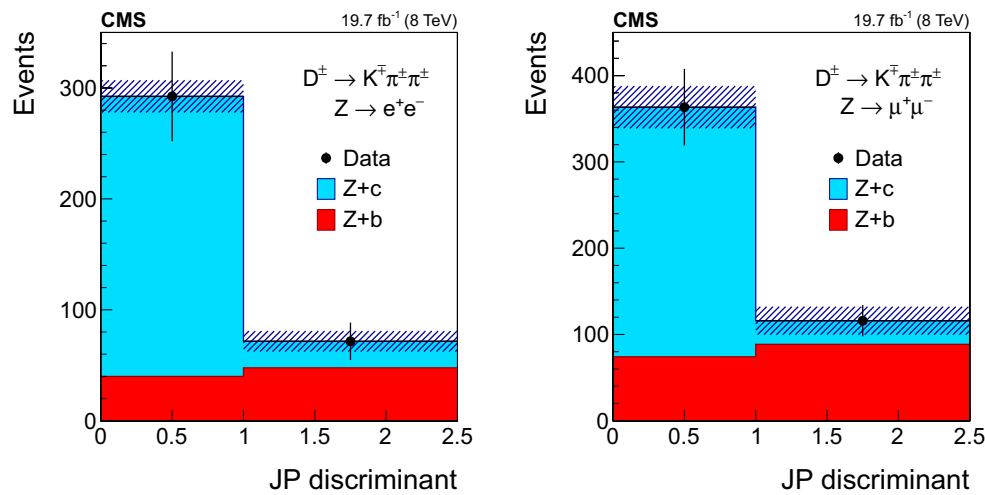
Fig. 8 Background-subtracted distributions of the JP discriminant in the dielectron (left) and dimuon (right) channels for $Z + jets$ events with a $D^{\pm} \to K^{\mp}\pi^{\pm}\pi^{\pm}$ candidate. The shape of the $Z+c$ and $Z+b$ contributions is estimated as explained in the text. Their normalization is adjusted to the result of the signal extraction fit. Vertical bars on

data points represent the statistical uncertainty in the data. The hatched areas represent the sum in quadrature of the statistical uncertainties of the templates describing the two contributions ($Z+c$ from $W+c$ data events and $Z+b$ from simulation)
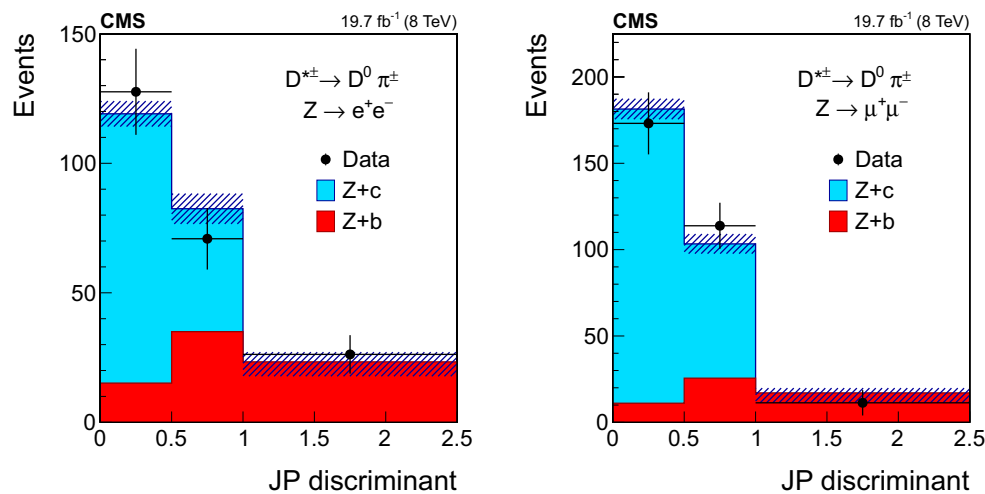
Fig. 9 Background-subtracted distributions of the JP discriminant in the dielectron (left) and dimuon (right) channels for $Z + jets$ events with a $D^*(2010)^{\pm} \to D^0\pi^{\pm} \to K^{\mp}\pi^{\pm}\pi^{\pm}$ candidate. The shape of the $Z+c$ and $Z+b$ contributions is estimated as explained in the text. Their normalization is adjusted to the result of the signal extraction fit.

Vertical bars on data points represent the statistical uncertainty in the data. The hatched areas represent the sum in quadrature of the statistical uncertainties of the templates describing the two contributions ($Z+c$ from $W+c$ data events and $Z+b$ from simulation)

all weakly decaying charm hadrons is 0.086 ± 0.004 [51,52]. The average of these two values, $\mathcal{B}(c \to \ell) = 0.091 \pm 0.003$, is consistent with the PYTHIA value used in our simulations (9.3%). We assign a 5% uncertainty in order to cover both central values within one standard deviation. The average of the inclusive b quark semileptonic branching fractions is $\mathcal{B}(b \to \ell) = 0.1069 \pm 0.0022$ [51], which is consistent with the PYTHIA value used in our simulations (10.5%). The corresponding uncertainty of 2% is propagated. The 5% sys-

tematic uncertainty in $\mathcal{B}(c \to \ell)$ is further propagated for the fraction of $Z + b$ events with a lepton in the final state through the decay chain $b \to c \to \ell$. Uncertainties in the branching ratios of other b hadron decay modes with a lepton in the final state, such as b hadron $\to \tau (\to \ell + X) + X'$, b hadron $\to J/\psi (\to \ell^+\ell^-) + X$, are not included since the expected contribution to the selected sample is negligible.

Since the simulation in the $D^{\pm}$ and $D^*(2010)^{\pm}$ modes is reweighted to match the experimental values [52], the uncer-
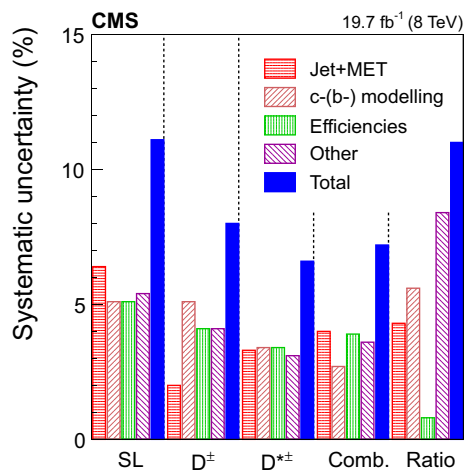
Fig. 10 Contributions to the systematic uncertainty in the measured $Z+c$ cross section and in the $(Z+c)/(Z+b)$ cross section ratio. The first three blocks in the graph show the uncertainties in the $Z+c$ cross section in the three decay modes, semileptonic (SL), $D^\pm$, and $D^*(2010)^\pm$, calculated from the combination of the dimuon and dielectron Z boson decay channels. The fourth block shows the systematic uncertainties in the combined (Comb.) $Z+c$ cross section. The last block presents the systematic uncertainty in the $(Z+c)/(Z+b)$ cross section ratio measured in the semileptonic mode. For every block, the height of the hatched bars indicates the contribution from the different sources of systematic uncertainty. The last, solid bar shows their sum in quadrature

tainty in the reweighting factors (5% for $D^\pm$ and 3.2% for $D^*(2010)^\pm$) is propagated to the cross section.

The contribution from gluon splitting processes to $Z+c$ production in the phase space of the measurement is small, and its possible mismodelling has little impact on the measurements. Its effect is evaluated with the simulated sample by independently increasing the weight of the events with at least two c (b) quarks in the list of generated particles close to the selected jet ($\Delta R(\text{jet}, c(b)) < 0.5$) by three times the experimental uncertainty in the gluon splitting rate into $c\bar{c}$, $b\bar{b}$ quark pairs [60,61].

The effects of the uncertainty in the jet energy scale and jet energy resolution are assessed by varying the corresponding jet energy scale (jet energy resolution) correction factors within their uncertainties according to the results of dedicated CMS studies [42,43]. The uncertainty from a mismeasurement of the missing transverse energy in the event is estimated by propagating the jet energy scale uncertainties and by adding 10% of the energy unassociated with reconstructed PF objects to the reconstructed E_T^{miss}.

The uncertainty in the c tagging scale factors is in the range 3.5–4%, and it is around 2.5% for the b tagging efficiency. In the $D^*(2010)^\pm$ mode, the candidate reconstruction procedure is repeated by independently changing by one standard deviation, in terms of the p_T resolution, the different p_T-thresholds imposed and the decay length significance requirement. We assume the uncertainty is the quadratic sum of the respective

differences between data and simulation in the change of the number of $D^*(2010)^\pm$ candidates (2.8%).

The uncertainty in the lepton efficiency correction factors is 4% in the $Z \to e^+e^-$ and 2% in the $Z \to \mu^+\mu^-$ channels. The uncertainty in the efficiency for the identification of muons inside jets is approximately 3%, according to dedicated studies in multijet events [20].

An additional systematic uncertainty is assigned to account for a possible mismodelling of the subtracted backgrounds. For the $t\bar{t}$ background the uncertainty is taken as the difference between the estimate based on data, as described in Sect. 6, and the one based on simulation. For $Z+$light flavour events, the systematic uncertainty is evaluated by using the MC correction factors associated with different misidentification probabilities. Finally, the diboson contribution is varied by the difference between the theoretical cross sections calculated at NNLO and NLO ($\approx 15\%$) [62–64].

The reference signal simulated sample is generated with MADGRAPH +PYTHIA6 using the PDF CTEQ6L1 and reweighted to NNLO PDF set MSTW2008NNLO. The difference resulting from using other NNLO PDF sets is small ($\lesssim 1\%$). Following the prescription of the PDF groups, the PDF uncertainty is of the same order.

The shapes of the discriminant distributions obtained from the W+c event sample are observed to be very stable. Changes in the jet energy scale and variations in the p_T threshold imposed to select W boson candidates do not affect the shape of the templates. The correction factors applied in certain regions to the corrected secondary-vertex mass template for $Z+b$ events are varied within their uncertainties.

Uncertainties due to the pileup modelling are calculated using a modified pileup profile obtained with a pp inelastic cross section changed by its estimated uncertainty, 6%. The uncertainty in the determination of the integrated luminosity of the data sample is 2.6% [65].

Systematic uncertainties in the differential $Z+c$ cross section and in the $(Z+c)/(Z+b)$ cross section ratio are in the range 11–15%. The main sources of systematic uncertainty in the differential distributions are due to the jet energy scale determination, the charm fractions for c hadron production and decay in simulation, and the efficiencies of heavy flavour tagging. The uncertainty in the binned c tagging efficiency scaling factors is 7–8%. Uncertainties in the b tagging efficiencies are 3–5%. An additional source of systematic uncertainty in the differential measurement as a function of the transverse momentum of the jet arises from the statistical uncertainty in the determination of the response matrix used to correct for migration of events across p_T^{jet} bins, as described in Sect. 9. Its impact is evaluated by repeating the correction procedure using a large number of response matrices, built from the nominal one by varying its components according to their statistical uncertainties. The effect is in the

range 4–6% for the Z + c cross section and 4.5–7% for the (Z + c)/(Z + b) cross section ratio.

8 Inclusive Z + c cross section and (Z + c)/(Z + b) cross section ratio

For all channels under study, the Z + c cross section is determined in the fiducial region $p_T^\ell > 20\,\mathrm{GeV}$, $|\eta^\ell| < 2.1$, $71 < m_{\ell\ell} < 111\,\mathrm{GeV}$, $p_T^{\mathrm{jet}} > 25\,\mathrm{GeV}$, $|\eta^{\mathrm{jet}}| < 2.5$, and $\Delta R(\mathrm{jet}, \ell) > 0.5$, using the following expression:

$$\sigma(\mathrm{Z+c})\,\mathcal{B} = \frac{N_{\mathrm{Z+c}}^{\mathrm{signal}}}{\mathcal{C}\,\mathcal{L}}, \tag{1}$$

where $N_{\mathrm{Z+c}}^{\mathrm{signal}}$ is the fitted yield of Z + c events and $\mathcal{L}$ is the integrated luminosity. The factor $\mathcal{C}$ corrects for event losses in the selection process and is estimated using simulated events. The $\mathcal{C}$ factors also include the relevant branching fraction for the corresponding channel.

Similarly, the ratio of cross sections $\sigma(\mathrm{Z+c})/\sigma(\mathrm{Z+b})$ is calculated in the same fiducial region applying the previous expression also for the Z + b contribution:

$$\frac{\sigma(\mathrm{Z+c})}{\sigma(\mathrm{Z+b})} = \frac{N_{\mathrm{Z+c}}^{\mathrm{signal}}}{N_{\mathrm{Z+b}}^{\mathrm{signal}}} \frac{\mathcal{C}(\mathrm{Z+b})}{\mathcal{C}(\mathrm{Z+c})}, \tag{2}$$

Table 1 shows the Z + c production cross section obtained in the three modes and the (Z + c)/(Z + b) cross section ratio (semileptonic mode only).

For the three categories of this analysis the Z + c cross sections obtained in the dielectron and dimuon Z boson decay channels are consistent. The results obtained in the three analysis categories are also consistent. Several combinations are performed to improve the precision of the measurement taking into account statistical and systematic uncertainties of the individual measurements. Systematic uncertainties arising from a common source and affecting several measurements are considered as fully correlated. In particular, all systematic uncertainties are assumed fully correlated between the electron and muon channels, except those related to lepton reconstruction. The average Z + c cross sections obtained in the three categories, together with the combination of the six measurements, are presented in Table 1. The combination is dominated by the result in the semileptonic mode. The contribution of the D*(2010)$^\pm$ mode to the average is also significant despite the limited size of the selected samples.

The cross section ratio $\sigma(\mathrm{Z+c})/\sigma(\mathrm{Z+b})$ has been measured in the semileptonic mode, in the two Z boson decay channels, and the results among them are consistent. Both cross section ratios are combined taking into account the statistical and systematic uncertainties in the two channels, and

the correlations among them. The combination is given in Table 1.

The measured Z + c cross section and the (Z + c)/(Z + b) cross section ratio are compared to theoretical predictions obtained using two MC event generators and the MCFM program.

A prediction of the Z + c fiducial cross section is obtained with the MADGRAPH sample. It is estimated by applying the phase space definition requirements to generator level quantities: two leptons from the Z boson decay with $p_T^\ell > 20\,\mathrm{GeV}$, $|\eta^\ell| < 2.1$, and dilepton invariant mass in the range $71 < m_{\ell\ell} < 111\,\mathrm{GeV}$; a generator-level c jet with $p_T^{\mathrm{c\,jet}} > 25\,\mathrm{GeV}$, $|\eta^{\mathrm{c\,jet}}| < 2.5$ and separated from the leptons by a distance $\Delta R(\mathrm{c\,jet}, \ell) > 0.5$. A prediction of the Z + b cross section, and hence of the (Z + c)/(Z + b) cross section ratio, is similarly derived applying the relevant phase space definition requirements to b flavoured generator-level jets.

The MADGRAPH prediction, $\sigma(\mathrm{Z+c})\,\mathcal{B} = 8.14 \pm 0.03\,\mathrm{(stat)} \pm 0.25\,\mathrm{(PDF)}$ pb, is in agreement with the measured value. The quoted PDF uncertainty corresponds to the largest difference in the predictions obtained using the central members of two different PDF sets (MSTW2008 vs NNPDF2.3); uncertainties computed using their respective PDF error sets are about half this value.

We have also compared the measurements with predictions obtained with a sample of events generated with MADGRAPH5_aMC@NLO v2.2.1 [66] (hereafter denoted as MG5_aMC) generator interfaced with PYTHIA v8.212 [67] using the CUETP8M1 tune [68] for parton showering and hadronization. The matrix element calculation includes the Z boson production process with 0, 1, and 2 partons at NLO. The FxFx [69] merging scheme between jets from matrix element and parton showers is implemented with a merging scale parameter set to 20 GeV. The NNPDF3.0 PDF set [70] is used for the matrix element calculation, while the NNPDF2.3 LO is used for the showering and hadronization.

The MG5_aMC prediction of the Z + c cross section is slightly higher, $\sigma(\mathrm{Z+c})\,\mathcal{B} = 9.46 \pm 0.04\,\mathrm{(stat)} \pm 0.15\,\mathrm{(PDF)} \pm 0.50\,\mathrm{(scales)}$ pb, but still in agreement with the measurement. Uncertainties in the prediction are evaluated using the reweighting features implemented in the generator [71]. The quoted PDF uncertainty corresponds to the standard deviation of the predictions obtained using the one hundred replicas in the NNPDF3.0 PDF set. The scale uncertainty is the envelope of the predictions when the factorization and renormalization scales are varied by a factor of two or one half independently, always keeping the ratio between them less than or equal to two.

Theoretical predictions in perturbative quantum chromodynamics at NLO for the associated production of a Z boson and at least one c quark are obtained with the MCFM 7.0 program [72]. Several sets of NLO PDF sets are used, accessed

through the LHAPDF6 [73] library interface. Partons are clustered into jets using the anti-k_T algorithm with a distance parameter of 0.5. The kinematic requirements follow the experimental selection: the two leptons from the Z boson decay with $p_T^\ell > 20$ GeV, $|\eta^\ell| < 2.1$, $71 < m_{\ell\ell} < 111$ GeV and a c parton jet with $p_T^{\text{parton jet}} > 25$ GeV, $|\eta^{\text{parton jet}}| < 2.5$, and separated from the leptons by $\Delta R(\text{parton jet}, \ell) > 0.5$. The factorization and renormalization scales are set to the mass of the Z boson. The PDF uncertainty in the predictions is evaluated following the prescription recommended by the individual PDF groups; the scale uncertainty is estimated as the envelope of the results with (twice, half) factorization and renormalization scales variations.

The prediction computed with MCFM follows the calculation reported in Refs. [72,74]. The leading contribution gc → Zc is evaluated at NLO including virtual and real corrections. Some of these corrections feature two jets in the final state, one of them with heavy flavour quark content. The calculation also includes the process q$\bar{\text{q}}$ → Zc$\bar{\text{c}}$ evaluated at LO, where either one of the heavy flavour quarks escapes detection or the two of them coalesce into a single jet.

The MCFM prediction, which is a parton-level calculation, is corrected for hadronization effects so it can be compared with the particle-level measurements reported in this paper. The correction factor is computed with the MADGRAPH simulated sample comparing the predicted cross section using generator-level jets and parton jets. Parton jets are defined using the same anti-k_T clustering algorithm with a distance parameter of 0.5, applied to all quarks and gluons after showering, but before hadronization. The flavour assignment for parton jets follows similar criteria as for generator-level jets: a parton jet is labelled as a b jet if there is at least a b quark among its constituents, regardless of the presence of any c or light quarks. It is classified as c jet if there is at least a c quark, and no b quark, among the constituents, and light otherwise. The size of the correction is ≈ 10% for Z+c and ≈ 15% for Z+b cross sections, in good agreement with the estimation in Ref. [75].

After the hadronization correction the MCFM prediction still misses contributions from the parton shower evolution, underlying event, and multiple parton interactions. An approximate value of the total correction due to these processes and hadronization is estimated using MADGRAPH and amounts to ≈ 30%. This correction is not applied to MCFM predictions, but can explain the observed differences between MCFM and the predictions of other generators.

Predictions are produced using MSTW08 and CT10 PDF sets and a recent PDF set from the NNPDF Collaboration, NNPDF3IC [76], where the charm quark PDF is no longer assumed to be perturbatively generated through pair production from gluons and light quarks, but is parameterized and

determined along with the light quark and gluon PDFs. The PDF set where the charm quark PDF is generated perturbatively, NNPDF3nIC [76], is also used.

No differences in the predictions are observed using either NNPDF3IC or NNPDF3nIC PDF sets. Differences among them start to be sizeable when the transverse momentum of the Z boson is $\gtrsim 100$ GeV [76]. The largest prediction is obtained using the MSTW08 PDF set, $\sigma(Z + c)\,\mathcal{B} = 5.32 \pm 0.01$ (stat) $^{+0.12}_{-0.06}$ (PDF) $^{+0.34}_{-0.38}$ (scales) pb. Predictions obtained using CT10 and NNPDF3IC are 5% smaller than with MSTW08. The uncertainties in all the calculations are of the same order.

The MADGRAPH prediction for the (Z+c)/(Z+b) cross section ratio is 1.781 ± 0.006 (stat) ± 0.004 (PDF), where the PDF uncertainty reflects the largest variation using the various PDF sets. The expectation from MG5_aMC is 1.84 ± 0.01 (stat) ± 0.07 (scales). The uncertainties from the several members within one PDF set essentially vanish in the ratio. Both predictions agree with the measured ratio.

A prediction for the cross section ratio is also obtained with MCFM, as the ratio of the predictions for $\sigma(Z + c)$ and $\sigma(Z + b)$, using the same parameters emulating the experimental scenario for both processes. The calculation of the $\sigma(Z + b)$ cross section follows the same reference as $\sigma(Z + c)$ [72,74]. The highest predicted value is $\sigma(Z + c)/\sigma(Z + b) = 1.58 \pm 0.01$ (stat+PDF syst) ± 0.07 (scales) obtained when the CT10 PDF set is used. The prediction from NNPDF3IC is about 10% lower, mainly because the predicted Z + b cross section using this PDF is the highest one.

9 Differential Z+c cross section and (Z+c)/(Z+b) cross section ratio

The Z + c production cross section and the (Z+c)/(Z+b) cross section ratio are measured differentially as a function of the transverse momentum of the Z boson, p_T^Z, and of the transverse momentum of the HF jet with the sample selected in the semileptonic mode described in Sect. 4.1. The transverse momentum of the Z boson is reconstructed from the momenta of the two selected leptons. The sample is divided into three different subsamples according to the value of the variable of interest, p_T^Z or p_T^{jet}, and the fit procedure is performed independently for each of them and for each Z boson decay mode. The number and size of the bins is chosen such that the corrected secondary-vertex mass distribution for each bin is sufficiently populated to perform the signal extraction fit.

Potential effects of event migration between neighbouring bins and inside/outside the acceptance due to the detector resolution are studied using simulated samples. A detector

response matrix is built with those events fulfilling the selection criteria both with generated and reconstructed variables. The element (i, j) in the matrix determines the probability that an event with generated p_T^Z (p_T^{jet}) in bin i ends up reconstructed in bin j of the distribution.

Migration effects in p_T^Z are found to be negligible and no correction is applied. An uncertainty of 1%, which corresponds to the difference between the cross sections with and without corrections, is included in the systematic uncertainties.

Some migration of events between neighbouring bins in p_T^{jet} is expected because of the energy resolution, mainly between the first and second bins ($< 30\%$), while migrations between the second and third bins are less than 10%. Migration effects are expected to be the same in the two Z boson decay modes. The response matrix is used to unfold the fitted signal yields to actual signal yields at particle level. Events with a generated p_T^{jet} outside the fiducial region and reconstructed inside it because of resolution effects are subtracted prior to the unfolding procedure. Corrections are made for acceptance losses at the border of the kinematical region because of the detector resolution and reconstruction inefficiencies. The unfolding is performed with an analytical inversion of the matrix defining the event migrations. Statistical and systematic uncertainties are propagated through the unfolding procedure.

Tables 2 and 3 summarize the fitted Z + c and Z + b signal yields, the Z + c cross section, and the (Z + c)/(Z + b) cross section ratio in the three p_T^Z and p_T^{jet} bins and in the two Z boson decay channels. The differential cross section and cross section ratio measured in the two Z boson decay channels are consistent and are combined to obtain the final results, taking into account the statistical and systematic uncertainties in the two channels and the correlations among them. The combined cross section and cross section ratio are presented in Table 4. They are also shown graphically in Fig. 11 in bins of p_T^Z (top) and p_T^{jet} (bottom).

Theoretical predictions for the differential cross section and cross section ratio are also obtained with the two MC generator programs and with MCFM. They are shown in Fig. 11 for comparison with the measured values. The uncertainties in the MADGRAPH predictions include the statistical and PDF uncertainties. Scale variations are additionally included in the uncertainties of MG5_aMC and MCFM. Predictions from MG5_aMC are higher than the predictions from MADGRAPH in the three bins of the Z + c differential distributions. A higher (Z + c)/(Z + b) cross section ratio is predicted up to 60 GeV, although consistent within uncertainties. The predictions from MADGRAPH and MG5_aMC successfully reproduce the measurements. The level of agreement is similar in terms of the Z + c cross section and the (Z + c)/(Z + b) cross section ratio.

A similar ordering appears in the differential cross sections and the inclusive cross sections for theoretical predictions calculated with MCFM and the various PDF sets. The highest Z + c cross section is predicted using the MSTW08 PDF set, the largest differential (Z + c)/(Z + b) cross section ratio in the two variables is obtained with the CT10 PDF set. All MCFM predictions are lower than the differential cross section measurements as a function of p_T^Z. This discrepancy is most pronounced in the first bin in p_T^{jet}. Differences between predictions and data are reduced in the (Z + c)/(Z + b) cross section ratio comparison.

The fitted charm PDF in NNPDF3IC [76] set is consistent with having an intrinsic component. The fitted fraction of the proton momentum that the charm quark component carries is $(0.7 \pm 0.3)\%$ if EMC data [77] is included in the fit and $(1.6 \pm 1.2)\%$ without it. After subtraction of the perturbative component, the momentum fraction of the proton carried by the IC component is $(0.5 \pm 0.3)\%$ if EMC data is included in the fit, or $(1.4 \pm 1.2)\%$ if not. Upper limits from the CTEQ-TEA Collaboration are also available [78,79]. Quoted limits on the proton momentum fraction carried by the IC component vary between 1.5 and 2.5% at 90% confidence level depending on the parameterization used.

If the proton momentum fraction taken by the charm quark component (intrinsic + perturbative) is of order $\approx 2\%$, an increase in the production of Z + c events with a $p_T^Z \approx 100$ GeV of at least 20–25% would be expected [76]. Should it be smaller than 1%, the cross section increase would be limited in the p_T^Z region around 100–200 GeV and only become visible at significantly higher p_T^Z ($\gtrsim 500$ GeV). The measured cross section in the p_T^Z bin [60, 200] GeV is in agreement with predictions from MADGRAPH and MG5_aMC using a perturbative charm quark PDF. This measurement is in agreement with no increase in the production rate or with a very modest one, as expected from current upper limits on the IC component. No increase in the production rate in the highest p_T^{jet} bin is observed, either.

10 Summary

The associated production of a Z boson with at least one charm quark jet in proton-proton collisions at a centre-of-mass energy of 8 TeV was studied with a data sample corresponding to an integrated luminosity of 19.7 ± 0.5 fb^{-1}. It was compared to the production of a Z boson with at least one b quark jet. Selection of event candidates relies on the identification of semileptonic decays of c or b hadrons with a muon in the final state and through the reconstruction of exclusive decay channels of D$^\pm$ and D*(2010)$^\pm$ mesons. The Z boson is identified through its decay into an e$^+$e$^-$ or $\mu^+\mu^-$ pair.

Table 2 Differential cross section $\mathrm{d}\sigma(Z+c)/\mathrm{d}p_T^Z\,\mathcal{B}$ and cross section ratio $(\mathrm{d}\sigma(Z+c)/\mathrm{d}p_T^Z)/(\mathrm{d}\sigma(Z+b)/\mathrm{d}p_T^Z)$ in the semileptonic mode and in the two Z boson decay channels. The $N_{Z+c}^{\mathrm{signal}}$ and $N_{Z+b}^{\mathrm{signal}}$ are the yields of Z+c and Z+b events, respectively, extracted from the fit. All uncertainties quoted in the table are statistical, except for those of the measured cross sections and cross section ratios, where the first uncertainty is statistical and the second is the estimated systematic uncertainty from the sources discussed in the text

Channel	$N_{Z+c}^{\mathrm{signal}}$	$\frac{\mathrm{d}\sigma(Z+c)}{\mathrm{d}p_T^Z}\mathcal{B}$ [pb]	$N_{Z+b}^{\mathrm{signal}}$	$\frac{\mathrm{d}\sigma(Z+c)}{\mathrm{d}p_T^Z}/\frac{\mathrm{d}\sigma(Z+b)}{\mathrm{d}p_T^Z}$
$0 < p_T^Z < 30\,\mathrm{GeV}$				
$Z \to e^+e^-$	212 ± 44	$0.067 \pm 0.014 \pm 0.010$	578 ± 52	$1.5 \pm 0.4 \pm 0.2$
$Z \to \mu^+\mu^-$	380 ± 61	$0.102 \pm 0.016 \pm 0.017$	693 ± 68	$2.7 \pm 0.6 \pm 0.4$
$30 < p_T^Z < 60\,\mathrm{GeV}$				
$Z \to e^+e^-$	501 ± 60	$0.144 \pm 0.017 \pm 0.019$	1035 ± 66	$2.4 \pm 0.4 \pm 0.3$
$Z \to \mu^+\mu^-$	586 ± 92	$0.123 \pm 0.019 \pm 0.017$	1422 ± 87	$1.9 \pm 0.4 \pm 0.3$
$60 < p_T^Z < 200\,\mathrm{GeV}$				
$Z \to e^+e^-$	363 ± 53	$0.017 \pm 0.002 \pm 0.002$	913 ± 67	$1.7 \pm 0.3 \pm 0.2$
$Z \to \mu^+\mu^-$	474 ± 73	$0.017 \pm 0.003 \pm 0.002$	1056 ± 81	$2.0 \pm 0.4 \pm 0.3$

Table 3 Differential cross section $\mathrm{d}\sigma(Z+c)/\mathrm{d}p_T^{\mathrm{jet}}\,\mathcal{B}$ and cross section ratio $(\mathrm{d}\sigma(Z+c)/\mathrm{d}p_T^{\mathrm{jet}})/(\mathrm{d}\sigma(Z+b)/\mathrm{d}p_T^{\mathrm{jet}})$ in the semileptonic mode and in the two Z boson decay channels. The $N_{Z+c}^{\mathrm{signal}}$ and $N_{Z+b}^{\mathrm{signal}}$ are the yields of Z+c and Z+b events, respectively, extracted from the fit. All uncertainties quoted in the table are statistical, except for those of the measured cross sections and cross section ratios, where the first uncertainty is statistical and the second is the estimated systematic uncertainty from the sources discussed in the text

Channel	$N_{Z+c}^{\mathrm{signal}}$	$\frac{\mathrm{d}\sigma(Z+c)}{\mathrm{d}p_T^{\mathrm{jet}}}\mathcal{B}$ [pb]	$N_{Z+b}^{\mathrm{signal}}$	$\frac{\mathrm{d}\sigma(Z+c)}{\mathrm{d}p_T^{\mathrm{jet}}}/\frac{\mathrm{d}\sigma(Z+b)}{\mathrm{d}p_T^{\mathrm{jet}}}$
$25 < p_T^{\mathrm{jet}} < 40\,\mathrm{GeV}$				
$Z \to e^+e^-$	476 ± 58	$0.342 \pm 0.048 \pm 0.041$	1022 ± 67	$2.7 \pm 0.6 \pm 0.3$
$Z \to \mu^+\mu^-$	583 ± 91	$0.337 \pm 0.059 \pm 0.055$	1393 ± 90	$2.4 \pm 0.6 \pm 0.4$
$40 < p_T^{\mathrm{jet}} < 60\,\mathrm{GeV}$				
$Z \to e^+e^-$	289 ± 47	$0.090 \pm 0.027 \pm 0.018$	843 ± 59	$1.3 \pm 0.4 \pm 0.2$
$Z \to \mu^+\mu^-$	456 ± 66	$0.104 \pm 0.027 \pm 0.014$	1044 ± 75	$1.9 \pm 0.5 \pm 0.3$
$60 < p_T^{\mathrm{jet}} < 200\,\mathrm{GeV}$				
$Z \to e^+e^-$	311 ± 56	$0.012 \pm 0.003 \pm 0.008$	686 ± 64	$1.7 \pm 0.5 \pm 0.3$
$Z \to \mu^+\mu^-$	369 ± 63	$0.013 \pm 0.003 \pm 0.007$	800 ± 75	$1.9 \pm 0.5 \pm 0.3$

Table 4 Differential Z+c cross section and (Z+c)/(Z+b) cross section ratio. The first column presents the p_T range for each bin. Column 2 presents the cross section and column 3 the ratio. The differential measurements as a function of the transverse momentum of the Z boson (jet with heavy flavour content) are given in the upper (lower) part of the table. The first uncertainty is statistical and the second is the systematic uncertainty arising from the sources discussed in the text

$[p_{T\,\mathrm{min}}^Z, p_{T\,\mathrm{max}}^Z]$[GeV]	$\frac{\mathrm{d}\sigma(Z+c)}{\mathrm{d}p_T^Z}\mathcal{B}$ [pb]	$\frac{\mathrm{d}\sigma(Z+c)}{\mathrm{d}p_T^Z}/\frac{\mathrm{d}\sigma(Z+b)}{\mathrm{d}p_T^Z}$
$[0, 30]$	$0.077 \pm 0.011 \pm 0.011$	$1.7 \pm 0.3 \pm 0.2$
$[30, 60]$	$0.133 \pm 0.013 \pm 0.017$	$2.1 \pm 0.3 \pm 0.3$
$[60, 200]$	$0.017 \pm 0.002 \pm 0.002$	$1.8 \pm 0.3 \pm 0.2$
$[p_{T\,\mathrm{min}}^{\mathrm{jet}}, p_{T\,\mathrm{max}}^{\mathrm{jet}}]$[GeV]	$\frac{\mathrm{d}\sigma(Z+c)}{\mathrm{d}p_T^{\mathrm{jet}}}\mathcal{B}$ [pb]	$\frac{\mathrm{d}\sigma(Z+c)}{\mathrm{d}p_T^{\mathrm{jet}}}/\frac{\mathrm{d}\sigma(Z+b)}{\mathrm{d}p_T^{\mathrm{jet}}}$
$[25, 40]$	$0.341 \pm 0.037 \pm 0.040$	$2.5 \pm 0.4 \pm 0.3$
$[40, 60]$	$0.097 \pm 0.019 \pm 0.012$	$1.5 \pm 0.3 \pm 0.2$
$[60, 200]$	$0.013 \pm 0.002 \pm 0.002$	$1.8 \pm 0.4 \pm 0.2$
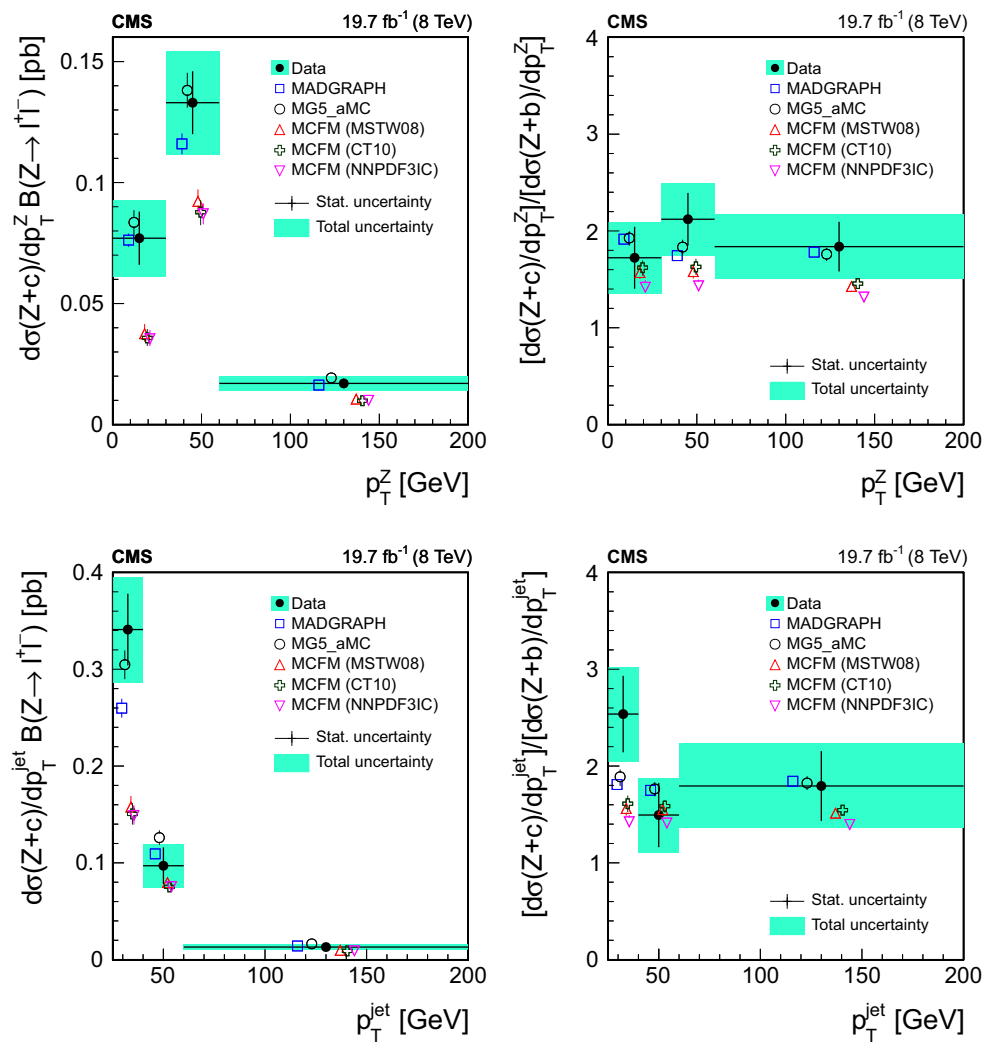
Fig. 11 Differential Z+c cross section and (Z+c)/(Z+b) cross section ratio as a function of the transverse momentum of the Z boson (top) and the transverse momentum of the jet (bottom). The combination of the results in the dielectron and dimuon channels is presented. The Z+c differential cross section is shown on the left and the (Z+c)/(Z+b) cross section ratio is on the right. Statistical uncertainties in the data are shown as crosses. The solid rectangles indicate the total (statistical and systematic) experimental uncertainty. Statistical and systematic uncertainties in the theoretical predictions are shown added in quadrature. Symbols showing the theoretical expectations are slightly displaced from the bin centre in the horizontal axis for better visibility of the predictions

The cross section for the production of a Z boson associated with at least one c quark jet is measured. The measurement is performed in the kinematic region with two leptons with transverse momentum $p_T^\ell > 20$ GeV, pseudorapidity $|\eta^\ell| < 2.1$, dilepton invariant mass $71 < m_{\ell\ell} < 111$ GeV and a jet with $p_T^{\text{jet}} > 25$ GeV, $|\eta^{\text{jet}}| < 2.5$, separated from the leptons of the Z boson candidate by a distance $\Delta R(\text{jet}, \ell) > 0.5$.

The Z + c production cross sections measured in all the analysis categories are fully consistent, and the combined value is $\sigma(pp \rightarrow Z+c+X)\mathcal{B}(Z \rightarrow \ell^+\ell^-) = 8.8 \pm 0.5$ (stat)± 0.6 (syst) pb. This is the first measurement at the LHC of Z+c production in the central pseudorapidity region.

The cross section ratio for the production of a Z boson and at least one c and at least one b quark jet is measured in the same kinematic region and is $\sigma(pp \rightarrow Z+c+X)/\sigma(pp \rightarrow Z+b+X) = 2.0 \pm 0.2$ (stat) ± 0.2 (syst).

The size of the sample selected in the semileptonic channel allows for the first differential measurements of the Z+c cross section at the LHC. The Z+c cross section and (Z+c)/(Z+b) cross section ratio are measured as a function of the transverse momentum of the Z boson and of the heavy flavour jet.

The measurements are in agreement with the leading order predictions from MADGRAPH and next-to-leading-order predictions from MADGRAPH5_aMC@NLO. Predictions from the MCFM program are lower than the measured Z + c cross

section and $(Z+c)/(Z+b)$ cross section ratio, both inclusively and differentially. This difference can be explained by the absence of parton shower development and nonperturbative effects in the MCFM calculation.

Measurements in the highest p_T^Z (p_T^{jet}) region analyzed, $60 < p_T^Z(p_T^{jet}) < 200$ GeV, would be sensitive to the existence of an intrinsic charm component inside the proton if this IC component were large enough to induce a significant enhancement in the $Z+c$ production cross section. However, our measurements of the $Z+c$ cross section and $(Z+c)/(Z+b)$ cross section ratio are consistent with predictions using PDF sets with no IC component.

References

1. ATLAS Collaboration, Search for pair-produced third-generation squarks decaying via charm quarks or in compressed supersymmetric scenarios in pp collisions at $\sqrt{s} = 8$ TeV with the ATLAS detector. Phys. Rev. D **90**, 052008 (2014). https://doi.org/10.1103/PhysRevD.90.052008. arXiv:1407.0608

2. ATLAS Collaboration, Search for Scalar Charm Quark Pair Production in pp Collisions at $\sqrt{s} = 8$ TeV with the ATLAS Detector. Phys. Rev. Lett. **114**, 161801 (2015). https://doi.org/10.1103/PhysRevLett.114.161801. arXiv:1501.01325

3. CMS Collaboration, Searches for third-generation squark production in fully hadronic final states in proton-proton collisions at $\sqrt{s} = 8$ TeV. JHEP **06**, 116 (2015). https://doi.org/10.1007/JHEP06(2015)116. arXiv:1503.08037

4. CMS Collaboration, Search for the standard model Higgs boson decaying to bottom quarks in pp collisions at $\sqrt{s} = 7$ TeV. Phys. Lett. B **710**, 284 (2012). https://doi.org/10.1016/j.physletb.2012.02.085. arXiv:1202.4195

5. CMS Collaboration, Search for the standard model Higgs boson produced in association with a W or a Z boson and decaying to bottom quarks. Phys. Rev. D **89**, 012003 (2014). https://doi.org/10.1103/PhysRevD.89.012003. arXiv:1310.3687

6. ATLAS Collaboration, Search for the standard model Higgs boson produced in association with a vector boson and decaying to a b-quark pair with the ATLAS detector. Phys. Lett. B **718**, 369 (2012). https://doi.org/10.1016/j.physletb.2012.10.061. arXiv:1207.0210

7. ATLAS Collaboration, Search for the b$\bar{b}$ decay of the standard model Higgs boson in associated (W/Z)H production with the ATLAS detector. JHEP **01**, 069 (2015). https://doi.org/10.1007/JHEP01(2015)069. arXiv:1409.6212

8. C. Delaunay, T. Golling, G. Perez, Y. Soreq, Enhanced Higgs boson coupling to charm pairs. Phys. Rev. D **89**, 033014 (2014). https://doi.org/10.1103/PhysRevD.89.033014. arXiv:1310.7029

9. S.J. Brodsky et al., A review of the intrinsic heavy quark content of the nucleon. Adv. High Energy Phys. **2015**, 231547 (2015). https://doi.org/10.1155/2015/231547. arXiv:1504.06287

10. P.-H. Beauchemin, V.A. Bednyakov, G.I. Lykasov, YuYu. Stepanenko, Search for intrinsic charm in vector boson production accompanied by heavy-flavor jets. Phys. Rev. D **92**, 034014 (2015). https://doi.org/10.1103/PhysRevD.92.034014. arXiv:1410.2616

11. G. Bailas, V.P. Goncalves, Phenomenological implications of the intrinsic charm in the Z boson production at the LHC. Eur. Phys. J. C **76**, 105 (2016). https://doi.org/10.1140/epjc/s10052-016-3941-z. arXiv:1512.06007

12. A.V. Lipatov, G.I. Lykasov, YuYu. Stepanenko, V.A. Bednyakov, Probing proton intrinsic charm in photon or Z boson production accompanied by heavy jets at the LHC. Phys. Rev. D **94**, 053011 (2016). https://doi.org/10.1103/PhysRevD.94.053011. arXiv:1606.04882

13. T. Boettcher, P. Ilten, M. Williams, Direct probe of the intrinsic charm content of the proton. Phys. Rev. D **93**, 074008 (2016). https://doi.org/10.1103/PhysRevD.93.074008. arXiv:1512.06666

14. D0 Collaboration, Measurement of associated production of Z bosons with charm quark jets in p$\bar{p}$ collisions at $\sqrt{s} = 1.96$ TeV. Phys. Rev. Lett. **112**, 042001 (2014). https://doi.org/10.1103/PhysRevLett.112.042001. arXiv:1308.4384

15. CDF Collaboration, Measurement of vector boson plus $D^*(2010)^+$ meson production in $\bar{p}p$ collisions at $\sqrt{s} = 1.96$ TeV. Phys. Rev. D **93**, 052012 (2016). https://doi.org/10.1103/PhysRevD.93.052012. arXiv:1508.06980

16. LHCb Collaboration, Observation of associated production of a Z boson with a D meson in the forward region. JHEP **04**, 091 (2014). https://doi.org/10.1007/JHEP04(2014)091. arXiv:1401.3245

17. CMS Collaboration, Measurements of the associated production of a Z boson and b jets in pp collisions at $\sqrt{s} = 8$ TeV. Eur. Phys. J. C **77**, 751 (2017). https://doi.org/10.1140/epjc/s10052-017-5140-y. arXiv:1611.06507

18. CMS Collaboration, Description and performance of track and primary-vertex reconstruction with the CMS tracker. JINST **9**, P10009 (2014). https://doi.org/10.1088/1748-0221/9/10/P10009. arXiv:1405.6569

19. CMS Collaboration, Performance of electron reconstruction and selection with the CMS detector in proton-proton collisions at $\sqrt{s} = 8$ TeV. JINST **10**, P06005 (2015). https://doi.org/10.1088/1748-0221/10/06/P06005. arXiv:1502.02701

20. CMS Collaboration, Performance of CMS muon reconstruction in pp collision events at $\sqrt{s} = 7$ TeV. JINST **7**, P10002 (2012). https://doi.org/10.1088/1748-0221/7/10/P10002. arXiv:1206.4071

21. CMS Collaboration, The CMS trigger system. JINST **12**, P01020 (2017). https://doi.org/10.1088/1748-0221/12/01/P01020. arXiv:1609.02366

22. CMS Collaboration, The CMS experiment at the CERN LHC. JINST **3**, S08004 (2008). https://doi.org/10.1088/1748-0221/3/08/S08004

23. J. Alwall et al., Madgraph 5: going beyond. JHEP **06**, 128 (2011). https://doi.org/10.1007/JHEP06(2011)128. arXiv:1106.0522

24. T. Sjöstrand, S. Mrenna, P.Z. Skands, PYTHIA 6.4 physics and manual. JHEP **05**, 026 (2006). https://doi.org/10.1088/1126-6708/2006/05/026. arXiv:hep-ph/0603175

25. J. Alwall et al., Comparative study of various algorithms for the merging of parton showers and matrix elements in hadronic collisions. Eur. Phys. J. C **53**, 473 (2008). https://doi.org/10.1140/epjc/s10052-007-0490-5. arXiv:0706.2569

26. J. Alwall, S. de Visscher, F. Maltoni, QCD radiation in the production of heavy colored particles at the LHC. JHEP **02**, 017 (2009). https://doi.org/10.1088/1126-6708/2009/02/017. arXiv:0810.5350

27. J. Pumplin et al., New generation of parton distributions with uncertainties from global QCD analysis. JHEP **07**, 012 (2002). https://doi.org/10.1088/1126-6708/2002/07/012. arXiv:hep-ph/0201195

28. J.M. Campbell, R.K. Ellis, P. Nason, E. Re, Top-pair production and decay at NLO matched with parton showers. JHEP **04**, 114 (2015). https://doi.org/10.1007/JHEP04(2015)114. arXiv:1412.1828

29. P. Nason, A new method for combining NLO QCD with shower Monte Carlo algorithms. JHEP **11**, 040 (2004). https://doi.org/10.1088/1126-6708/2004/11/040. arXiv:hep-ph/0409146

30. S. Frixione, P. Nason, C. Oleari, Matching NLO QCD computations with parton shower simulations: the POWHEG method. JHEP **11**, 070 (2007). https://doi.org/10.1088/1126-6708/2007/11/070. arXiv:0709.2092

31. S. Alioli, P. Nason, C. Oleari, E. Re, A general framework for implementing NLO calculations in shower Monte Carlo programs: the POWHEG BOX. JHEP **06**, 043 (2010). https://doi.org/10.1007/JHEP06(2010)043. arXiv:1002.2581

32. J. Gao et al., CT10 next-to-next-to-leading order global analysis of QCD. Phys. Rev. D **89**, 033009 (2014). https://doi.org/10.1103/PhysRevD.89.033009. arXiv:1302.6246

33. CMS Collaboration, Study of the underlying event at forward rapidity in pp collisions at $\sqrt{s} = 0.9, 2.76,$ and 7 TeV. JHEP **04**, 072 (2013). https://doi.org/10.1007/JHEP04(2013)072, arXiv:1302.2394

34. GEANT4 Collaboration, GEANT4—a simulation toolkit. Nucl. Instrum. Methods A **506**, 250 (2003). https://doi.org/10.1016/S0168-9002(03)01368-8

35. Y. Li, F. Petriello, Combining QCD and electroweak corrections to dilepton production in the framework of the FEWZ simulation code. Phys. Rev. D **86**, 094034 (2012). https://doi.org/10.1103/PhysRevD.86.094034. arXiv:1208.5967

36. A.D. Martin, W.J. Stirling, R.S. Thorne, G. Watt, Parton distributions for the LHC. Eur. Phys. J. C **63**, 189 (2009). https://doi.org/10.1140/epjc/s10052-009-1072-5. arXiv:0901.0002

37. J.M. Campbell, R. Ellis, MCFM for the Tevatron and the LHC. Nucl. Phys. B Proc. Suppl. **205**, 10 (2010). https://doi.org/10.1016/j.nuclphysbps.2010.08.011. arXiv:1007.3492

38. M. Czakon, P. Fiedler, A. Mitov, Total top-quark pair-production cross-section at hadron colliders through $\mathcal{O}(\alpha_S^4)$. Phys. Rev. Lett. **110**, 252004 (2013). https://doi.org/10.1103/PhysRevLett.110.252004. arXiv:1303.6254

39. CMS Collaboration, Measurement of the inclusive W and Z production cross sections in pp collisions at $\sqrt{s} = 7$ TeV with the CMS experiment. JHEP **10**, 132 (2011). https://doi.org/10.1007/JHEP10(2011)132. arXiv:1107.4789

40. CMS Collaboration, Particle-flow reconstruction and global event description with the CMS detector. JINST **12**, P10003 (2017). https://doi.org/10.1088/1748-0221/12/10/P10003. arXiv:1706.04965

41. M. Cacciari, G.P. Salam, G. Soyez, The anti-k_t jet clustering algorithm. JHEP **04**, 063 (2008). https://doi.org/10.1088/1126-6708/2008/04/063. arXiv:0802.1189

42. CMS Collaboration, Determination of jet energy calibration and transverse momentum resolution in CMS. JINST **6**, P11002 (2011). https://doi.org/10.1088/1748-0221/6/11/P11002. arXiv:1107.4277

43. CMS Collaboration, Jet energy scale and resolution in the CMS experiment in pp collisions at 8 TeV. JINST **12**, P02014 (2017). https://doi.org/10.1088/1748-0221/12/02/P02014. arXiv:1607.03663

44. CMS Collaboration, MET performance in 8 TeV data. CMS Physics Analysis Summary CMS-PAS-JME-12-002 (2013). http://cds.cern.ch/record/1543527

45. M. Cacciari, G.P. Salam, Pileup subtraction using jet areas. Phys. Lett. B **659**, 119 (2008). https://doi.org/10.1016/j.physletb.2007.09.077. arXiv:0707.1378

46. CMS Collaboration, Measurements of differential production cross sections for a Z boson in association with jets in pp collisions at $\sqrt{s} = 8$ TeV. JHEP **04**, 022 (2017). https://doi.org/10.1007/JHEP04(2017)022. arXiv:1611.03844

47. CMS Collaboration, Identification of b-quark jets with the CMS experiment. JINST **8**, P04013 (2013). https://doi.org/10.1088/1748-0221/8/04/P04013. arXiv:1211.4462

48. CMS Collaboration, Measurement of b$\bar{\text{b}}$ angular correlations based on secondary vertex reconstruction at $\sqrt{s} = 7$ TeV. JHEP **03**, 136 (2011). https://doi.org/10.1007/JHEP03(2011)136. arXiv:1102.3194

49. CMS Collaboration, Measurement of the cross section and angular correlations for associated production of a Z boson with b hadrons in pp collisions at $\sqrt{s} = 7$ TeV. JHEP **12**, 039 (2013). https://doi.org/10.1007/JHEP12(2013)039. arXiv:1310.1349

50. W. Waltenberger, R. Frühwirth, P. Vanlaer, Adaptive vertex fitting. J. Phys. G **34**, N343 (2007). https://doi.org/10.1088/0954-3899/34/12/N01

51. Particle Data Group Collaboration, Review of Particle Physics. Chin. Phys. C **40**, 100001 (2016). https://doi.org/10.1088/1674-1137/40/10/100001

52. L. Gladilin, Fragmentation fractions of c and b quarks into charmed hadrons at LEP. Eur. Phys. J. C **75**, 19 (2015). https://doi.org/10.1140/epjc/s10052-014-3250-3. arXiv:1404.3888

53. O.P.A.L. Collaboration, Measurement of f(c → D^{*+}X), f(b → D^{*+}X) and Γ(c$\bar{c}$)/Γ(had) using D$^{*\pm}$ mesons. Eur. Phys. J. C **1**, 439 (1998). https://doi.org/10.1007/s100520050095. arXiv:hep-ex/9708021

54. ALEPH Collaboration, Study of charm production in Z decays. Eur. Phys. J. C **16**, 597 (2000). https://doi.org/10.1007/s100520000421. arXiv:hep-ex/9909032

55. DELPHI Collaboration, Determination of P(c → D^{*+}) and BR(c → ℓ$^+$) at LEP 1. Eur. Phys. J. C **12** 209 (2000). https://doi.org/10.1007/s100529900227

56. R. Frühwirth, R. Kubinec, W. Mitaroff, M. Regler, Vertex reconstruction and track bundling at the LEP collider using robust algorithms. Comp. Phys. Commun. **96**, 189 (1996). https://doi.org/10.1016/0010-4655(96)00040-9

57. CMS Collaboration, Measurement of associated W+charm production in pp collisions at $\sqrt{s}$ = 7 TeV. JHEP **02**, 013 (2014). https://doi.org/10.1007/JHEP02(2014)013. arXiv:1310.1138

58. CMS Collaboration, Performance of b tagging at $\sqrt{s}$ = 8 TeV in multijet, ttbar and boosted topology events. CMS Physics Analysis Summary CMS-PAS-BTV-13-001 (2013)

59. LHCb Collaboration, Identification of beauty and charm quark jets at LHCb. JINST **10**, P06013 (2015). https://doi.org/10.1088/1748-0221/10/06/P06013. arXiv:1504.07670

60. ALEPH Collaboration, A measurement of the gluon splitting rate into c$\bar{c}$ pairs in hadronic Z decays. Phys. Lett. B **561**, 213 (2003). https://doi.org/10.1016/S0370-2693(03)00495-7. arXiv:hep-ex/0302003

61. ALEPH Collaboration, A measurement of the gluon splitting rate into b$\bar{b}$ pairs in hadronic Z decays. Phys. Lett. B **434**, 437 (1998). https://doi.org/10.1016/S0370-2693(98)00850-8

62. T. Gehrmann et al., W$^+$W$^-$ production at hadron colliders in next to next to leading order QCD. Phys. Rev. Lett. **113**, 212001 (2014). https://doi.org/10.1103/PhysRevLett.113.212001. arXiv:1408.5243

63. F. Cascioli et al., ZZ production at hadron colliders in NNLO QCD. Phys. Lett. B **735**, 311 (2014). https://doi.org/10.1016/j.physletb.2014.06.056. arXiv:1405.2219

64. M. Grazzini, S. Kallweit, D. Rathlev, M. Wiesemann, W$^{\pm}$Z production at hadron colliders in NNLO QCD. Phys. Lett. B **761**, 179 (2016). https://doi.org/10.1016/j.physletb.2016.08.017. arXiv:1604.08576

65. CMS Collaboration, CMS Luminosity Based on Pixel Cluster Counting - Summer 2013 Update. CMS Physics Analysis Summary CMS-PAS-LUM-13-001 (2013). http://cds.cern.ch/record/1598864

66. J. Alwall et al., The automated computation of tree-level and next-to-leading order differential cross sections, and their matching to parton shower simulations. JHEP **07**, 079 (2014). https://doi.org/10.1007/JHEP07(2014)079. arXiv:1405.0301

67. T. Sjöstrand, S. Mrenna, P.Z. Skands, A brief introduction to PYTHIA 8.1. Comput. Phys. Commun. **178**, 852 (2008). https://doi.org/10.1016/j.cpc.2008.01.036. arXiv:0710.3820

68. CMS Collaboration, Event generator tunes obtained from underlying event and multiparton scattering measurements. Eur. Phys. J. C **76**, 155 (2016). https://doi.org/10.1140/epjc/s10052-016-3988-x. arXiv:1512.00815

69. R. Frederix, S. Frixione, Merging meets matching in MC@NLO. JHEP **12**, 061 (2012). https://doi.org/10.1007/JHEP12(2012)061. arXiv:1209.6215

70. NNPDF Collaboration, Parton distributions for the LHC Run II. JHEP **04**, 040 (2015). https://doi.org/10.1007/JHEP04(2015)040. arXiv:1410.8849

71. R. Frederix et al., Four-lepton production at hadron colliders: aMC@NLO predictions with theoretical uncertainties. JHEP **02**, 099 (2012). https://doi.org/10.1007/JHEP02(2012)099. arXiv:1110.4738

72. J.M. Campbell, R.K. Ellis, F. Maltoni, S. Willenbrock, Associated production of a Z boson and a single heavy-quark jet. Phys. Rev. D **69**, 074021 (2004). https://doi.org/10.1103/PhysRevD.69.074021. arXiv:hep-ph/0312024

73. A. Buckley et al., LHAPDF6: parton density access in the LHC precision era. Eur. Phys. J. C **75**, 132 (2015). https://doi.org/10.1140/epjc/s10052-015-3318-8. arXiv:1412.7420

74. J.M. Campbell, R.K. Ellis, F. Maltoni, S. Willenbrock, Higgs-boson production in association with a single bottom quark. Phys. Rev. D **67**, 095002 (2003). https://doi.org/10.1103/PhysRevD.67.095002. arXiv:hep-ph/0204093

75. CMS Collaboration, Measurement of the Z/γ*+b-jet cross section in pp collisions at $\sqrt{s}$ = 7 TeV. JHEP **06**, 126 (2012). https://doi.org/10.1007/JHEP06(2012)126. arXiv:1204.1643

76. NNPDF Collaboration, A determination of the charm content of the proton. Eur. Phys. J. C **76**, 647 (2016). https://doi.org/10.1140/epjc/s10052-016-4469-y. arXiv:1605.06515

77. European Muon Collaboration, Production of charmed particles in 250 GeV μ$^+$-iron interactions. Nucl. Phys. B **213**, 31 (1983). https://doi.org/10.1016/0550-3213(83)90174-8

78. S. Dulat et al., Intrinsic charm parton distribution functions from CTEQ-TEA global analysis. Phys. Rev. D **89**, 073004 (2014). https://doi.org/10.1103/PhysRevD.89.073004. arXiv:1309.0025

79. T.-J. Hou et al., Heavy flavors on CT14. in *Proceedings, 23rd International Workshop on Deep-Inelastic Scattering and Related Subjects* (DIS 2015), volume DIS2015 (Dallas, Texas, USA, 2015), p. 166

CMS Collaboration

Yerevan Physics Institute, Yerevan, Armenia

A. M. Sirunyan, A. Tumasyan

Institut für Hochenergiephysik, Wien, Austria

W. Adam, F. Ambrogi, E. Asilar, T. Bergauer, J. Brandstetter, E. Brondolin, M. Dragicevic, J. Erö, M. Flechl, M. Friedl, R. Frühwirth[1], V. M. Ghete, J. Grossmann, N. Hörmann, J. Hrubec, M. Jeitler[1], A. König, I. Krätschmer, D. Liko, T. Madlener, T. Matsushita, I. Mikulec, E. Pree, D. Rabady, N. Rad, H. Rohringer, J. Schieck[1], M. Spanring, D. Spitzbart, J. Strauss, W. Waltenberger, J. Wittmann, C.-E. Wulz[1], M. Zarucki

Institute for Nuclear Problems, Minsk, Belarus

V. Chekhovsky, V. Mossolov, J. Suarez Gonzalez

National Centre for Particle and High Energy Physics, Minsk, Belarus
N. Shumeiko

Universiteit Antwerpen, Antwerpen, Belgium
E. A. De Wolf, X. Janssen, J. Lauwers, M. Van De Klundert, H. Van Haevermaet, P. Van Mechelen, N. Van Remortel,
A. Van Spilbeeck

Vrije Universiteit Brussel, Brussel, Belgium
S. Abu Zeid, F. Blekman, J. D'Hondt, I. De Bruyn, J. De Clercq, K. Deroover, G. Flouris, S. Lowette, S. Moortgat,
L. Moreels, A. Olbrechts, Q. Python, K. Skovpen, S. Tavernier, W. Van Doninck, P. Van Mulders, I. Van Parijs

Université Libre de Bruxelles, Brussels, Belgium
H. Brun, B. Clerbaux, G. De Lentdecker, H. Delannoy, G. Fasanella, L. Favart, R. Goldouzian, A. Grebenyuk,
G. Karapostoli, T. Lenzi, J. Luetic, T. Maerschalk, A. Marinov, A. Randle-conde, T. Seva, C. Vander Velde, P. Vanlaer,
D. Vannerom, R. Yonamine, F. Zenoni, F. Zhang[2]

Ghent University, Ghent, Belgium
A. Cimmino, T. Cornelis, D. Dobur, A. Fagot, M. Gul, I. Khvastunov, D. Poyraz, S. Salva, R. Schöfbeck, M. Tytgat,
W. Van Driessche, W. Verbeke, N. Zaganidis

Université Catholique de Louvain, Louvain-la-Neuve, Belgium
H. Bakhshiansohi, O. Bondu, S. Brochet, G. Bruno, A. Caudron, S. De Visscher, C. Delaere, M. Delcourt, B. Francois,
A. Giammanco, A. Jafari, M. Komm, G. Krintiras, V. Lemaitre, A. Magitteri, A. Mertens, M. Musich, K. Piotrzkowski,
L. Quertenmont, M. Vidal Marono, S. Wertz

Université de Mons, Mons, Belgium
N. Beliy

Centro Brasileiro de Pesquisas Fisicas, Rio de Janeiro, Brazil
W. L. Aldá Júnior, F. L. Alves, G. A. Alves, L. Brito, C. Hensel, A. Moraes, M. E. Pol, P. Rebello Teles

Universidade do Estado do Rio de Janeiro, Rio de Janeiro, Brazil
E. Belchior Batista Das Chagas, W. Carvalho, J. Chinellato[3], A. Custódio, E. M. Da Costa, G. G. Da Silveira[4],
D. De Jesus Damiao, S. Fonseca De Souza, L. M. Huertas Guativa, H. Malbouisson, C. Mora Herrera, L. Mundim,
H. Nogima, A. Santoro, A. Sznajder, E. J. Tonelli Manganote[3], F. Torres Da Silva Araujo, A. Vilela Pereira

Universidade Estadual Paulista [a], Universidade Federal do ABC [b], São Paulo, Brazil
S. Ahuja[a], C. A. Bernardes[a], T. R. Fernandez Perez Tomei[a], E. M. Gregores[b], P. G. Mercadante[b], C. S. Moon[a],
S. F. Novaes[a], Sandra S. Padula[a], D. Romero Abad[b], J. C. Ruiz Vargas[a]

Institute for Nuclear Research and Nuclear Energy, Bulgarian Academy of Sciences, Sofia, Bulgaria
A. Aleksandrov, R. Hadjiiska, P. Iaydjiev, M. Misheva, M. Rodozov, S. Stoykova, G. Sultanov, M. Vutova

University of Sofia, Sofia, Bulgaria
A. Dimitrov, I. Glushkov, L. Litov, B. Pavlov, P. Petkov

Beihang University, Beijing, China
W. Fang[5], X. Gao[5]

Institute of High Energy Physics, Beijing, China
M. Ahmad, J. G. Bian, G. M. Chen, H. S. Chen, M. Chen, Y. Chen, C. H. Jiang, D. Leggat, Z. Liu, F. Romeo,
S. M. Shaheen, A. Spiezia, J. Tao, C. Wang, Z. Wang, E. Yazgan, H. Zhang, J. Zhao

State Key Laboratory of Nuclear Physics and Technology, Peking University, Beijing, China
Y. Ban, G. Chen, Q. Li, S. Liu, Y. Mao, S. J. Qian, D. Wang, Z. Xu

Universidad de Los Andes, Bogota, Colombia
C. Avila, A. Cabrera, L. F. Chaparro Sierra, C. Florez, C. F. González Hernández, J. D. Ruiz Alvarez

Faculty of Electrical Engineering, Mechanical Engineering and Naval Architecture, University of Split, Split, Croatia
N. Godinovic, D. Lelas, I. Puljak, P. M. Ribeiro Cipriano, T. Sculac

Faculty of Science, University of Split, Split, Croatia
Z. Antunovic, M. Kovac

Institute Rudjer Boskovic, Zagreb, Croatia
V. Brigljevic, D. Ferencek, K. Kadija, B. Mesic, T. Susa

University of Cyprus, Nicosia, Cyprus
M. W. Ather, A. Attikis, G. Mavromanolakis, J. Mousa, C. Nicolaou, F. Ptochos, P. A. Razis, H. Rykaczewski

Charles University, Prague, Czech Republic
M. Finger[6], M. Finger Jr.[6]

Universidad San Francisco de Quito, Quito, Ecuador
E. Carrera Jarrin

Academy of Scientific Research and Technology of the Arab Republic of Egypt, Egyptian Network of High Energy Physics, Cairo, Egypt
E. El-khateeb[7], S. Elgammal[8], A. Ellithi Kamel[9]

National Institute of Chemical Physics and Biophysics, Tallinn, Estonia
R. K. Dewanjee, M. Kadastik, L. Perrini, M. Raidal, A. Tiko, C. Veelken

Department of Physics, University of Helsinki, Helsinki, Finland
P. Eerola, J. Pekkanen, M. Voutilainen

Helsinki Institute of Physics, Helsinki, Finland
J. Härkönen, T. Järvinen, V. Karimäki, R. Kinnunen, T. Lampén, K. Lassila-Perini, S. Lehti, T. Lindén, P. Luukka, E. Tuominen, J. Tuominiemi, E. Tuovinen

Lappeenranta University of Technology, Lappeenranta, Finland
J. Talvitie, T. Tuuva

IRFU, CEA, Université Paris-Saclay, Gif-sur-Yvette, France
M. Besancon, F. Couderc, M. Dejardin, D. Denegri, J. L. Faure, F. Ferri, S. Ganjour, S. Ghosh, A. Givernaud, P. Gras, G. Hamel de Monchenault, P. Jarry, I. Kucher, E. Locci, M. Machet, J. Malcles, J. Rander, A. Rosowsky, M. Ö. Sahin, M. Titov

Laboratoire Leprince-Ringuet, Ecole polytechnique, CNRS/IN2P3-Université Paris-Saclay, Palaiseau, France
A. Abdulsalam, I. Antropov, S. Baffioni, F. Beaudette, P. Busson, L. Cadamuro, E. Chapon, C. Charlot, O. Davignon, R. Granier de Cassagnac, M. Jo, S. Lisniak, A. Lobanov, M. Nguyen, C. Ochando, G. Ortona, P. Paganini, P. Pigard, S. Regnard, R. Salerno, Y. Sirois, A. G. StahlLeiton, T. Strebler, Y. Yilmaz, A. Zabi

CNRS-IN2P3 IPHC UMR 7178, Université de Strasbourg, 67000 Strasbourg, France
J.-L. Agram[10], J. Andrea, D. Bloch, J.-M. Brom, M. Buttignol, E. C. Chabert, N. Chanon, C. Collard, E. Conte[10], X. Coubez, J.-C. Fontaine[10], D. Gelé, U. Goerlach, A.-C. Le Bihan, P. Van Hove

CNRS/IN2P3, Centre de Calcul de l'Institut National de Physique Nucleaire et de Physique des Particules, Villeurbanne, France
S. Gadrat

CNRS-IN2P3, Institut de Physique Nucléaire de Lyon, Université de Lyon, Université Claude Bernard Lyon 1, Villeurbanne, France
S. Beauceron, C. Bernet, G. Boudoul, R. Chierici, D. Contardo, B. Courbon, P. Depasse, H. El Mamouni, J. Fay, L. Finco, S. Gascon, M. Gouzevitch, G. Grenier, B. Ille, F. Lagarde, I. B. Laktineh, M. Lethuillier, L. Mirabito, A. L. Pequegnot, S. Perries, A. Popov[11], V. Sordini, M. Vander Donckt, S. Viret

Georgian Technical University, Tbilisi, Georgia
A. Khvedelidze[6]

Tbilisi State University, Tbilisi, Georgia
Z. Tsamalaidze[6]

I. Physikalisches Institut, RWTH Aachen University, Aachen, Germany

C. Autermann, S. Beranek, L. Feld, M. K. Kiesel, K. Klein, M. Lipinski, M. Preuten, C. Schomakers, J. Schulz, T. Verlage

III. Physikalisches Institut A, RWTH Aachen University, Aachen, Germany

A. Albert, M. Brodski, E. Dietz-Laursonn, D. Duchardt, M. Endres, M. Erdmann, S. Erdweg, T. Esch, R. Fischer, A. Güth, M. Hamer, T. Hebbeker, C. Heidemann, K. Hoepfner, S. Knutzen, M. Merschmeyer, A. Meyer, P. Millet, S. Mukherjee, M. Olschewski, K. Padeken, T. Pook, M. Radziej, H. Reithler, M. Rieger, F. Scheuch, L. Sonnenschein, D. Teyssier, S. Thüer

III. Physikalisches Institut B, RWTH Aachen University, Aachen, Germany

G. Flügge, B. Kargoll, T. Kress, A. Künsken, J. Lingemann, T. Müller, A. Nehrkorn, A. Nowack, C. Pistone, O. Pooth, A. Stahl[12]

Deutsches Elektronen-Synchrotron, Hamburg, Germany

M. Aldaya Martin, T. Arndt, C. Asawatangtrakuldee, K. Beernaert, O. Behnke, U. Behrens, A. A. Bin Anuar, K. Borras[13], V. Botta, A. Campbell, P. Connor, C. Contreras-Campana, F. Costanza, C. Diez Pardos, G. Eckerlin, D. Eckstein, T. Eichhorn, E. Eren, E. Gallo[14], J. Garay Garcia, A. Geiser, A. Gizhko, J. M. Grados Luyando, A. Grohsjean, P. Gunnellini, A. Harb, J. Hauk, M. Hempel[15], H. Jung, A. Kalogeropoulos, M. Kasemann, J. Keaveney, C. Kleinwort, I. Korol, D. Krücker, W. Lange, A. Lelek, T. Lenz, J. Leonard, K. Lipka, W. Lohmann[15], R. Mankel, I.-A. Melzer-Pellmann, A. B. Meyer, G. Mittag, J. Mnich, A. Mussgiller, E. Ntomari, D. Pitzl, R. Placakyte, A. Raspereza, B. Roland, M. Savitskyi, P. Saxena, R. Shevchenko, S. Spannagel, N. Stefaniuk, G. P. Van Onsem, R. Walsh, Y. Wen, K. Wichmann, C. Wissing

University of Hamburg, Hamburg, Germany

S. Bein, V. Blobel, M. Centis Vignali, A. R. Draeger, T. Dreyer, E. Garutti, D. Gonzalez, J. Haller, M. Hoffmann, A. Junkes, R. Klanner, R. Kogler, N. Kovalchuk, S. Kurz, T. Lapsien, I. Marchesini, D. Marconi, M. Meyer, M. Niedziela, D. Nowatschin, F. Pantaleo[12], T. Peiffer, A. Perieanu, C. Scharf, P. Schleper, A. Schmidt, S. Schumann, J. Schwandt, J. Sonneveld, H. Stadie, G. Steinbrück, F. M. Stober, M. Stöver, H. Tholen, D. Troendle, E. Usai, L. Vanelderen, A. Vanhoefer, B. Vormwald

Institut für Experimentelle Kernphysik, Karlsruhe, Germany

M. Akbiyik, C. Barth, S. Baur, C. Baus, J. Berger, E. Butz, R. Caspart, T. Chwalek, F. Colombo, W. De Boer, A. Dierlamm, B. Freund, R. Friese, M. Giffels, A. Gilbert, D. Haitz, F. Hartmann[12], S. M. Heindl, U. Husemann, F. Kassel[12], S. Kudella, H. Mildner, M. U. Mozer, Th. Müller, M. Plagge, G. Quast, K. Rabbertz, M. Schröder, I. Shvetsov, G. Sieber, H. J. Simonis, R. Ulrich, S. Wayand, M. Weber, T. Weiler, S. Williamson, C. Wöhrmann, R. Wolf

Institute of Nuclear and Particle Physics (INPP), NCSR Demokritos, Aghia Paraskevi, Greece

G. Anagnostou, G. Daskalakis, T. Geralis, V. A. Giakoumopoulou, A. Kyriakis, D. Loukas, I. Topsis-Giotis

National and Kapodistrian University of Athens, Athens, Greece

S. Kesisoglou, A. Panagiotou, N. Saoulidou

University of Ioánnina, Ioánnina, Greece

I. Evangelou, C. Foudas, P. Kokkas, N. Manthos, I. Papadopoulos, E. Paradas, J. Strologas, F. A. Triantis

MTA-ELTE Lendület CMS Particle and Nuclear Physics Group, Eötvös Loránd University, Budapest, Hungary

M. Csanad, N. Filipovic, G. Pasztor

Wigner Research Centre for Physics, Budapest, Hungary

G. Bencze, C. Hajdu, D. Horvath[16], F. Sikler, V. Veszpremi, G. Vesztergombi[17], A. J. Zsigmond

Institute of Nuclear Research ATOMKI, Debrecen, Hungary

N. Beni, S. Czellar, J. Karancsi[18], A. Makovec, J. Molnar, Z. Szillasi

Institute of Physics, University of Debrecen, Debrecen, Hungary

M. Bartók[17], P. Raics, Z. L. Trocsanyi, B. Ujvari

Indian Institute of Science (IISc), Bangalore, India

S. Choudhury, J. R. Komaragiri

National Institute of Science Education and Research, Bhubaneswar, India

S. Bahinipati[19], S. Bhowmik, P. Mal, K. Mandal, A. Nayak[20], D. K. Sahoo[19], N. Sahoo, S. K. Swain

Panjab University, Chandigarh, India

S. Bansal, S. B. Beri, V. Bhatnagar, U. Bhawandeep, R. Chawla, N. Dhingra, A. K. Kalsi, A. Kaur, M. Kaur, R. Kumar,
P. Kumari, A. Mehta, M. Mittal, J. B. Singh, G. Walia

University of Delhi, Delhi, India

Ashok Kumar, Aashaq Shah, A. Bhardwaj, S. Chauhan, B. C. Choudhary, R. B. Garg, S. Keshri, A. Kumar, S. Malhotra,
M. Naimuddin, K. Ranjan, R. Sharma, V. Sharma

Saha Institute of Nuclear Physics, HBNI, Kolkata, India

R. Bhardwaj, R. Bhattacharya, S. Bhattacharya, S. Dey, S. Dutt, S. Dutta, S. Ghosh, N. Majumdar, A. Modak, K. Mondal,
S. Mukhopadhyay, S. Nandan, A. Purohit, A. Roy, D. Roy, S. Roy Chowdhury, S. Sarkar, M. Sharan, S. Thakur

Indian Institute of Technology Madras, Madras, India

P. K. Behera

Bhabha Atomic Research Centre, Mumbai, India

R. Chudasama, D. Dutta, V. Jha, V. Kumar, A. K. Mohanty[12], P. K. Netrakanti, L. M. Pant, P. Shukla, A. Topkar

Tata Institute of Fundamental Research-A, Mumbai, India

T. Aziz, S. Dugad, B. Mahakud, S. Mitra, G. B. Mohanty, B. Parida, N. Sur, B. Sutar

Tata Institute of Fundamental Research-B, Mumbai, India

S. Banerjee, S. Bhattacharya, S. Chatterjee, P. Das, M. Guchait, Sa. Jain, S. Kumar, M. Maity[21], G. Majumder,
K. Mazumdar, T. Sarkar[21], N. Wickramage[22]

Indian Institute of Science Education and Research (IISER), Pune, India

S. Chauhan, S. Dube, V. Hegde, A. Kapoor, K. Kothekar, S. Pandey, A. Rane, S. Sharma

Institute for Research in Fundamental Sciences (IPM), Tehran, Iran

S. Chenarani[23], E. Eskandari Tadavani, S. M. Etesami[23], M. Khakzad, M. Mohammadi Najafabadi, M. Naseri,
S. Paktinat Mehdiabadi[24], F. Rezaei Hosseinabadi, B. Safarzadeh[25], M. Zeinali

University College Dublin, Dublin, Ireland

M. Felcini, M. Grunewald

INFN Sezione di Bari [a], Università di Bari [b], Politecnico di Bari [c], Bari, Italy

M. Abbrescia[a,b], C. Calabria[a,b], C. Caputo[a,b], A. Colaleo[a], D. Creanza[a,c], L. Cristella[a,b], N. De Filippis[a,c],
M. De Palma[a,b], L. Fiore[a], G. Iaselli[a,c], G. Maggi[a,c], M. Maggi[a], G. Miniello[a,b], S. My[a,b], S. Nuzzo[a,b], A. Pompili[a,b],
G. Pugliese[a,c], R. Radogna[a,b], A. Ranieri[a], G. Selvaggi[a,b], A. Sharma[a], L. Silvestris[a,12], R. Venditti[a], P. Verwilligen[a]

INFN Sezione di Bologna [a], Università di Bologna [b], Bologna, Italy

G. Abbiendi[a], C. Battilana, D. Bonacorsi[a,b], S. Braibant-Giacomelli[a,b], L. Brigliadori[a,b], R. Campanini[a,b],
P. Capiluppi[a,b], A. Castro[a,b], F. R. Cavallo[a], S. S. Chhibra[a,b], M. Cuffiani[a,b], G. M. Dallavalle[a], F. Fabbri[a], A. Fanfani[a,b],
D. Fasanella[a,b], P. Giacomelli[a], L. Guiducci[a,b], S. Marcellini[a], G. Masetti[a], F. L. Navarria[a,b], A. Perrotta[a], A. M. Rossi[a,b],
T. Rovelli[a,b], G. P. Siroli[a,b], N. Tosi[a,b,12]

INFN Sezione di Catania [a], Università di Catania [b], Catania, Italy

S. Albergo[a,b], S. Costa[a,b], A. Di Mattia[a], F. Giordano[a,b], R. Potenza[a,b], A. Tricomi[a,b], C. Tuve[a,b]

INFN Sezione di Firenze [a], Università di Firenze [b], Firenze, Italy

G. Barbagli[a], K. Chatterjee[a,b], V. Ciulli[a,b], C. Civinini[a], R. D'Alessandro[a,b], E. Focardi[a,b], P. Lenzi[a,b], M. Meschini[a],
S. Paoletti[a], L. Russo[a,26], G. Sguazzoni[a], D. Strom[a], L. Viliani[a,b,12]

INFN Laboratori Nazionali di Frascati, Frascati, Italy

L. Benussi, S. Bianco, F. Fabbri, D. Piccolo, F. Primavera[12]

INFN Sezione di Genova [a], Università di Genova [b], Genoa, Italy

V. Calvelli[a,b], F. Ferro[a], E. Robutti[a], S. Tosi[a,b]

INFN Sezione di Milano-Bicocca [a]**, Università di Milano-Bicocca** [b]**, Milan, Italy**

L. Brianza[a,b], F. Brivio[a,b], V. Ciriolo[a,b], M. E. Dinardo[a,b], S. Fiorendi[a,b], S. Gennai[a], A. Ghezzi[a,b], P. Govoni[a,b], M. Malberti[a,b], S. Malvezzi[a], R. A. Manzoni[a,b], D. Menasce[a], L. Moroni[a], M. Paganoni[a,b], K. Pauwels[a,b], D. Pedrini[a], S. Pigazzini[a,b,27], S. Ragazzi[a,b], T. Tabarelli de Fatis[a,b]

INFN Sezione di Napoli [a]**, Università di Napoli 'Federico II'** [b]**, Naples, Italy, Università della Basilicata** [c]**, Potenza, Italy, Università G. Marconi** [d]**, Rome, Italy**

S. Buontempo[a], N. Cavallo[a,c], S. Di Guida[a,d,12], F. Fabozzi[a,c], F. Fienga[a,b], A. O. M. Iorio[a,b], W. A. Khan[a], L. Lista[a], S. Meola[a,d,12], P. Paolucci[a,15], C. Sciacca[a,b], F. Thyssen[a]

INFN Sezione di Padova [a]**, Università di Padova** [b]**, Padua, Italy, Università di Trento** [c]**, Trento, Italy**

P. Azzi[a,12], N. Bacchetta[a], M. Bellato[a], L. Benato[a,b], M. Benettoni[a], M. Biasotto[a,28], D. Bisello[a,b], A. Boletti[a,b], A. Carvalho Antunes De Oliveira[a,b], P. Checchia[a], M. Dall'Osso[a,b], P. De Castro Manzano[a], T. Dorigo[a], U. Dosselli[a], F. Gasparini[a,b], A. Gozzelino[a], S. Lacaprara[a], M. Margoni[a,b], A. T. Meneguzzo[a,b], N. Pozzobon[a,b], P. Ronchese[a,b], R. Rossin[a,b], E. Torassa[a], M. Zanetti[a,b], P. Zotto[a,b], G. Zumerle[a,b]

INFN Sezione di Pavia [a]**, Università di Pavia** [b]**, Pavia, Italy**

A. Braghieri[a], F. Fallavollita[a,b], A. Magnani[a,b], P. Montagna[a,b], S. P. Ratti[a,b], V. Re[a], M. Ressegotti, C. Riccardi[a,b], P. Salvini[a], I. Vai[a,b], P. Vitulo[a,b]

INFN Sezione di Perugia [a]**, Università di Perugia** [b]**, Perugia, Italy**

L. Alunni Solestizi[a,b], G. M. Bilei[a], D. Ciangottini[a,b], L. Fanò[a,b], P. Lariccia[a,b], R. Leonardi[a,b], G. Mantovani[a,b], V. Mariani[a,b], M. Menichelli[a], A. Saha[a], A. Santocchia[a,b], D. Spiga

INFN Sezione di Pisa [a]**, Università di Pisa** [b]**, Scuola Normale Superiore di Pisa** [c]**, Pisa, Italy**

K. Androsov[a], P. Azzurri[a,12], G. Bagliesi[a], J. Bernardini[a], T. Boccali[a], L. Borrello, R. Castaldi[a], M. A. Ciocci[a,b], R. Dell'Orso[a], G. Fedi[a], A. Giassi[a], M. T. Grippo[a,26], F. Ligabue[a,c], T. Lomtadze[a], L. Martini[a,b], A. Messineo[a,b], F. Palla[a], A. Rizzi[a,b], A. Savoy-Navarro[a,29], P. Spagnolo[a], R. Tenchini[a], G. Tonelli[a,b], A. Venturi[a], P. G. Verdini[a]

INFN Sezione di Roma [a]**, Sapienza Università di Roma** [b]**, Rome, Italy**

L. Barone[a,b], F. Cavallari[a], M. Cipriani[a,b], N. Daci[a], D. Del Re[a,b,12], M. Diemoz[a], S. Gelli[a,b], E. Longo[a,b], F. Margaroli[a,b], B. Marzocchi[a,b], P. Meridiani[a], G. Organtini[a,b], R. Paramatti[a,b], F. Preiato[a,b], S. Rahatlou[a,b], C. Rovelli[a], F. Santanastasio[a,b]

INFN Sezione di Torino [a]**, Università di Torino** [b]**, Torino, Italy, Università del Piemonte Orientale** [c]**, Novara, Italy**

N. Amapane[a,b], R. Arcidiacono[a,c,12], S. Argiro[a,b], M. Arneodo[a,c], N. Bartosik[a], R. Bellan[a,b], C. Biino[a], N. Cartiglia[a], F. Cenna[a,b], M. Costa[a,b], R. Covarelli[a,b], A. Degano[a,b], N. Demaria[a], B. Kiani[a,b], C. Mariotti[a], S. Maselli[a], E. Migliore[a,b], V. Monaco[a,b], E. Monteil[a,b], M. Monteno[a], M. M. Obertino[a,b], L. Pacher[a,b], N. Pastrone[a], M. Pelliccioni[a], G. L. Pinna Angioni[a,b], F. Ravera[a,b], A. Romero[a,b], M. Ruspa[a,c], R. Sacchi[a,b], K. Shchelina[a,b], V. Sola[a], A. Solano[a,b], A. Staiano[a], P. Traczyk[a,b]

INFN Sezione di Trieste [a]**, Università di Trieste** [b]**, Trieste, Italy**

S. Belforte[a], M. Casarsa[a], F. Cossutti[a], G. Della Ricca[a,b], A. Zanetti[a]

Kyungpook National University, Daegu, Korea

D. H. Kim, G. N. Kim, M. S. Kim, J. Lee, S. Lee, S. W. Lee, Y. D. Oh, S. Sekmen, D. C. Son, Y. C. Yang

Chonbuk National University, Jeonju, Korea

A. Lee

Institute for Universe and Elementary Particles, Chonnam National University, Kwangju, Korea

H. Kim, D. H. Moon

Hanyang University, Seoul, Korea

J. A. Brochero Cifuentes, J. Goh, T. J. Kim

Korea University, Seoul, Korea

S. Cho, S. Choi, Y. Go, D. Gyun, S. Ha, B. Hong, Y. Jo, Y. Kim, K. Lee, K. S. Lee, S. Lee, J. Lim, S. K. Park, Y. Roh

Seoul National University, Seoul, Korea

J. Almond, J. Kim, H. Lee, S. B. Oh, B. C. Radburn-Smith, S. H. Seo, U. K. Yang, H. D. Yoo, G. B. Yu

University of Seoul, Seoul, Korea

M. Choi, H. Kim, J. H. Kim, J. S. H. Lee, I. C. Park, G. Ryu

Sungkyunkwan University, Suwon, Korea

Y. Choi, C. Hwang, J. Lee, I. Yu

Vilnius University, Vilnius, Lithuania

V. Dudenas, A. Juodagalvis, J. Vaitkus

National Centre for Particle Physics, Universiti Malaya, Kuala Lumpur, Malaysia

I. Ahmed, Z. A. Ibrahim, M. A. B. Md Ali[30], F. Mohamad Idris[31], W. A. T. Wan Abdullah, M. N. Yusli, Z. Zolkapli

Centro de Investigacion y de Estudios Avanzados del IPN, Mexico City, Mexico

H. Castilla-Valdez, E. De La Cruz-Burelo, I. Heredia-De La Cruz[32], R. Lopez-Fernandez, J. Mejia Guisao,
A. Sanchez-Hernandez

Universidad Iberoamericana, Mexico City, Mexico

S. Carrillo Moreno, C. Oropeza Barrera, F. Vazquez Valencia

Benemerita Universidad Autonoma de Puebla, Puebla, Mexico

I. Pedraza, H. A. Salazar Ibarguen, C. Uribe Estrada

Universidad Autónoma de San Luis Potosí, San Luis Potosí, Mexico

A. Morelos Pineda

University of Auckland, Auckland, New Zealand

D. Krofcheck

University of Canterbury, Christchurch, New Zealand

P. H. Butler

National Centre for Physics, Quaid-I-Azam University, Islamabad, Pakistan

A. Ahmad, M. Ahmad, Q. Hassan, H. R. Hoorani, A. Saddique, M. A. Shah, M. Shoaib, M. Waqas

National Centre for Nuclear Research, Swierk, Poland

H. Bialkowska, M. Bluj, B. Boimska, T. Frueboes, M. Górski, M. Kazana, K. Nawrocki, K. Romanowska-Rybinska,
M. Szleper, P. Zalewski

Faculty of Physics, Institute of Experimental Physics, University of Warsaw, Warsaw, Poland

K. Bunkowski, A. Byszuk[33], K. Doroba, A. Kalinowski, M. Konecki, J. Krolikowski, M. Misiura, M. Olszewski,
A. Pyskir, M. Walczak

Laboratório de Instrumentação e Física Experimental de Partículas, Lisbon, Portugal

P. Bargassa, C. Beirão Da Cruz E Silva, B. Calpas, A. Di Francesco, P. Faccioli, M. Gallinaro, J. Hollar, N. Leonardo,
L. Lloret Iglesias, M. V. Nemallapudi, J. Seixas, O. Toldaiev, D. Vadruccio, J. Varela

Joint Institute for Nuclear Research, Dubna, Russia

A. Baginyan, A. Golunov, I. Golutvin, V. Karjavin, V. Korenkov, G. Kozlov, A. Lanev, A. Malakhov, V. Matveev[34,35],
V. V. Mitsyn, V. Palichik, V. Perelygin, S. Shmatov, N. Skatchkov, V. Smirnov, B. S. Yuldashev[36], A. Zarubin, V. Zhiltsov

Petersburg Nuclear Physics Institute, Gatchina (St. Petersburg), Russia

Y. Ivanov, V. Kim[37], E. Kuznetsova[38], P. Levchenko, V. Murzin, V. Oreshkin, I. Smirnov, V. Sulimov, L. Uvarov,
S. Vavilov, A. Vorobyev

Institute for Nuclear Research, Moscow, Russia

Yu. Andreev, A. Dermenev, S. Gninenko, N. Golubev, A. Karneyeu, M. Kirsanov, N. Krasnikov, A. Pashenkov, D. Tlisov,
A. Toropin

Institute for Theoretical and Experimental Physics, Moscow, Russia

V. Epshteyn, V. Gavrilov, N. Lychkovskaya, V. Popov, I. Pozdnyakov, G. Safronov, A. Spiridonov, M. Toms, E. Vlasov, A. Zhokin

Moscow Institute of Physics and Technology, Moscow, Russia

T. Aushev, A. Bylinkin[35]

National Research Nuclear University 'Moscow Engineering Physics Institute' (MEPhI), Moscow, Russia

M. Chadeeva[39], R. Chistov[39], E. Tarkovskii

P.N. Lebedev Physical Institute, Moscow, Russia

V. Andreev, M. Azarkin[35], I. Dremin[35], M. Kirakosyan, A. Terkulov

Skobeltsyn Institute of Nuclear Physics, Lomonosov Moscow State University, Moscow, Russia

A. Baskakov, A. Belyaev, E. Boos, M. Dubinin[40], L. Dudko, A. Ershov, A. Gribushin, V. Klyukhin, O. Kodolova, I. Lokhtin, I. Miagkov, S. Obraztsov, S. Petrushanko, V. Savrin, A. Snigirev

Novosibirsk State University (NSU), Novosibirsk, Russia

V. Blinov[41], Y. Skovpen[41], D. Shtol[41]

State Research Center of Russian Federation, Institute for High Energy Physics, Protvino, Russia

I. Azhgirey, I. Bayshev, S. Bitioukov, D. Elumakhov, V. Kachanov, A. Kalinin, D. Konstantinov, V. Krychkine, V. Petrov, R. Ryutin, A. Sobol, S. Troshin, N. Tyurin, A. Uzunian, A. Volkov

Faculty of Physics and Vinca Institute of Nuclear Sciences, University of Belgrade, Belgrade, Serbia

P. Adzic[42], P. Cirkovic, D. Devetak, M. Dordevic, J. Milosevic, V. Rekovic

Centro de Investigaciones Energéticas Medioambientales y Tecnológicas (CIEMAT), Madrid, Spain

J. Alcaraz Maestre, M. Barrio Luna, M. Cerrada, N. Colino, B. De La Cruz, A. Delgado Peris, A. Escalante Del Valle, C. Fernandez Bedoya, J. P. Fernández Ramos, J. Flix, M. C. Fouz, P. Garcia-Abia, O. Gonzalez Lopez, S. Goy Lopez, J. M. Hernandez, M. I. Josa, A. Pérez-Calero Yzquierdo, J. Puerta Pelayo, A. Quintario Olmeda, I. Redondo, L. Romero, M. S. Soares

Universidad Autónoma de Madrid, Madrid, Spain

C. Albajar, J. F. de Trocóniz, M. Missiroli, D. Moran

Universidad de Oviedo, Oviedo, Spain

J. Cuevas, C. Erice, J. Fernandez Menendez, I. Gonzalez Caballero, J. R. González Fernández, E. Palencia Cortezon, S. Sanchez Cruz, I. Suárez Andrés, P. Vischia, J. M. Vizan Garcia

Instituto de Física de Cantabria (IFCA), CSIC-Universidad de Cantabria, Santander, Spain

I. J. Cabrillo, A. Calderon, B. Chazin Quero, E. Curras, M. Fernandez, J. Garcia-Ferrero, G. Gomez, A. Lopez Virto, J. Marco, C. Martinez Rivero, F. Matorras, J. Piedra Gomez, T. Rodrigo, A. Ruiz-Jimeno, L. Scodellaro, N. Trevisani, I. Vila, R. Vilar Cortabitarte

CERN, European Organization for Nuclear Research, Geneva, Switzerland

D. Abbaneo, E. Auffray, P. Baillon, A. H. Ball, D. Barney, M. Bianco, P. Bloch, A. Bocci, C. Botta, T. Camporesi, R. Castello, M. Cepeda, G. Cerminara, Y. Chen, D. d'Enterria, A. Dabrowski, V. Daponte, A. David, M. De Gruttola, A. De Roeck, E. Di Marco[43], M. Dobson, B. Dorney, T. du Pree, M. Dünser, N. Dupont, A. Elliott-Peisert, P. Everaerts, G. Franzoni, J. Fulcher, W. Funk, D. Gigi, K. Gill, F. Glege, D. Gulhan, S. Gundacker, M. Guthoff, P. Harris, J. Hegeman, V. Innocente, P. Janot, O. Karacheban[15], J. Kieseler, H. Kirschenmann, V. Knünz, A. Kornmayer[12], M. J. Kortelainen, M. Krammer[1], C. Lange, P. Lecoq, C. Lourenço, M. T. Lucchini, L. Malgeri, M. Mannelli, A. Martelli, F. Meijers, J. A. Merlin, S. Mersi, E. Meschi, P. Milenovic[44], F. Moortgat, M. Mulders, H. Neugebauer, S. Orfanelli, L. Orsini, L. Pape, E. Perez, M. Peruzzi, A. Petrilli, G. Petrucciani, A. Pfeiffer, M. Pierini, A. Racz, T. Reis, G. Rolandi[45], M. Rovere, H. Sakulin, J. B. Sauvan, C. Schäfer, C. Schwick, M. Seidel, A. Sharma, P. Silva, P. Sphicas[46], J. Steggemann, M. Stoye, M. Tosi, D. Treille, A. Triossi, A. Tsirou, V. Veckalns[47], G. I. Veres[17], M. Verweij, N. Wardle, W. D. Zeuner

Paul Scherrer Institut, Villigen, Switzerland
W. Bertl, K. Deiters, W. Erdmann, R. Horisberger, Q. Ingram, H. C. Kaestli, D. Kotlinski, U. Langenegger, T. Rohe, S. A. Wiederkehr

Institute for Particle Physics and Astrophysics (IPA), ETH Zurich, Zurich, Switzerland
F. Bachmair, L. Bäni, P. Berger, L. Bianchini, B. Casal, G. Dissertori, M. Dittmar, M. Donegà, C. Grab, C. Heidegger, D. Hits, J. Hoss, G. Kasieczka, T. Klijnsma, W. Lustermann, B. Mangano, M. Marionneau, P. Martinez Ruiz del Arbol, M. Masciovecchio, M. T. Meinhard, D. Meister, F. Micheli, P. Musella, F. Nessi-Tedaldi, F. Pandolfi, J. Pata, F. Pauss, G. Perrin, L. Perrozzi, M. Quittnat, M. Rossini, M. Schönenberger, L. Shchutska, A. Starodumov[48], V. R. Tavolaro, K. Theofilatos, M. L. Vesterbacka Olsson, R. Wallny, A. Zagozdzinska[33], D. H. Zhu

Universität Zürich, Zurich, Switzerland
T. K. Aarrestad, C. Amsler[49], L. Caminada, M. F. Canelli, A. De Cosa, S. Donato, C. Galloni, A. Hinzmann, T. Hreus, B. Kilminster, J. Ngadiuba, D. Pinna, G. Rauco, P. Robmann, D. Salerno, C. Seitz, Y. Yang, A. Zucchetta

National Central University, Chung-Li, Taiwan
V. Candelise, T. H. Doan, Sh. Jain, R. Khurana, M. Konyushikhin, C. M. Kuo, W. Lin, A. Pozdnyakov, S. S. Yu

National Taiwan University (NTU), Taipei, Taiwan
Arun Kumar, P. Chang, Y. H. Chang, Y. Chao, K. F. Chen, P. H. Chen, F. Fiori, W.-S. Hou, Y. Hsiung, Y. F. Liu, R.-S. Lu, M. Miñano Moya, E. Paganis, A. Psallidas, J. F. Tsai

Department of Physics, Faculty of Science, Chulalongkorn University, Bangkok, Thailand
B. Asavapibhop, K. Kovitanggoon, G. Singh, N. Srimanobhas

Physics Department, Science and Art Faculty, Çukurova University, Adana, Turkey
A. Adiguzel[50], F. Boran, S. Cerci[51], S. Damarseckin, Z. S. Demiroglu, C. Dozen, I. Dumanoglu, S. Girgis, G. Gokbulut, Y. Guler, I. Hos[52], E. E. Kangal[53], O. Kara, A. Kayis Topaksu, U. Kiminsu, M. Oglakci, G. Onengut[54], K. Ozdemir[55], D. Sunar Cerci[51], H. Topakli[56], S. Turkcapar, I. S. Zorbakir, C. Zorbilmez

Physics Department, Middle East Technical University, Ankara, Turkey
B. Bilin, G. Karapinar[57], K. Ocalan[58], M. Yalvac, M. Zeyrek

Bogazici University, Istanbul, Turkey
E. Gülmez, M. Kaya[59], O. Kaya[60], A. Yetkin[61]

Istanbul Technical University, Istanbul, Turkey
A. Cakir, K. Cankocak

Institute for Scintillation Materials of National Academy of Science of Ukraine, Kharkov, Ukraine
B. Grynyov

National Scientific Center, Kharkov Institute of Physics and Technology, Kharkov, Ukraine
L. Levchuk, P. Sorokin

University of Bristol, Bristol, UK
R. Aggleton, F. Ball, L. Beck, J. J. Brooke, D. Burns, E. Clement, D. Cussans, H. Flacher, J. Goldstein, M. Grimes, G. P. Heath, H. F. Heath, J. Jacob, L. Kreczko, C. Lucas, D. M. Newbold[62], S. Paramesvaran, A. Poll, T. Sakuma, S. Seif El Nasr-storey, D. Smith, V. J. Smith

Rutherford Appleton Laboratory, Didcot, UK
K. W. Bell, A. Belyaev[63], C. Brew, R. M. Brown, L. Calligaris, D. Cieri, D. J. A. Cockerill, J. A. Coughlan, K. Harder, S. Harper, E. Olaiya, D. Petyt, C. H. Shepherd-Themistocleous, A. Thea, I. R. Tomalin, T. Williams

Imperial College, London, UK
M. Baber, R. Bainbridge, O. Buchmuller, A. Bundock, S. Casasso, M. Citron, D. Colling, L. Corpe, P. Dauncey, G. Davies, A. De Wit, M. Della Negra, R. Di Maria, P. Dunne, A. Elwood, D. Futyan, Y. Haddad, G. Hall, G. Iles, T. James, R. Lane, C. Laner, L. Lyons, A.-M. Magnan, S. Malik, L. Mastrolorenzo, J. Nash, A. Nikitenko[48], J. Pela, M. Pesaresi, D. M. Raymond, A. Richards, A. Rose, E. Scott, C. Seez, S. Summers, A. Tapper, K. Uchida, M. Vazquez Acosta[64], T. Virdee[12], J. Wright, S. C. Zenz

Brunel University, Uxbridge, UK
J. E. Cole, P. R. Hobson, A. Khan, P. Kyberd, I. D. Reid, P. Symonds, L. Teodorescu, M. Turner

Baylor University, Waco, USA
A. Borzou, K. Call, J. Dittmann, K. Hatakeyama, H. Liu, N. Pastika

Catholic University of America, Washington, DC, USA
R. Bartek, A. Dominguez

The University of Alabama, Tuscaloosa, USA
A. Buccilli, S. I. Cooper, C. Henderson, P. Rumerio, C. West

Boston University, Boston, USA
D. Arcaro, A. Avetisyan, T. Bose, D. Gastler, D. Rankin, C. Richardson, J. Rohlf, L. Sulak, D. Zou

Brown University, Providence, USA
G. Benelli, D. Cutts, A. Garabedian, J. Hakala, U. Heintz, J. M. Hogan, K. H. M. Kwok, E. Laird, G. Landsberg, Z. Mao, M. Narain, J. Pazzini, S. Piperov, S. Sagir, R. Syarif

University of California, Davis, Davis, USA
R. Band, C. Brainerd, R. Breedon, D. Burns, M. Calderon De La Barca Sanchez, M. Chertok, J. Conway, R. Conway, P. T. Cox, R. Erbacher, C. Flores, G. Funk, M. Gardner, W. Ko, R. Lander, C. Mclean, M. Mulhearn, D. Pellett, J. Pilot, S. Shalhout, M. Shi, J. Smith, M. Squires, D. Stolp, K. Tos, M. Tripathi, Z. Wang

University of California, Los Angeles, USA
M. Bachtis, C. Bravo, R. Cousins, A. Dasgupta, A. Florent, J. Hauser, M. Ignatenko, N. Mccoll, D. Saltzberg, C. Schnaible, V. Valuev

University of California, Riverside, Riverside, USA
E. Bouvier, K. Burt, R. Clare, J. Ellison, J. W. Gary, S. M. A. Ghiasi Shirazi, G. Hanson, J. Heilman, P. Jandir, E. Kennedy, F. Lacroix, O. R. Long, M. Olmedo Negrete, M. I. Paneva, A. Shrinivas, W. Si, H. Wei, S. Wimpenny, B. R. Yates

University of California, San Diego, La Jolla, USA
J. G. Branson, G. B. Cerati, S. Cittolin, M. Derdzinski, R. Gerosa, A. Holzner, D. Klein, G. Kole, V. Krutelyov, J. Letts, I. Macneill, D. Olivito, S. Padhi, M. Pieri, M. Sani, V. Sharma, S. Simon, M. Tadel, A. Vartak, S. Wasserbaech[65], F. Würthwein, A. Yagil, G. Zevi Della Porta

Department of Physics, University of California, Santa Barbara, Santa Barbara, USA
N. Amin, R. Bhandari, J. Bradmiller-Feld, C. Campagnari, A. Dishaw, V. Dutta, M. Franco Sevilla, C. George, F. Golf, L. Gouskos, J. Gran, R. Heller, J. Incandela, S. D. Mullin, A. Ovcharova, H. Qu, J. Richman, D. Stuart, I. Suarez, J. Yoo

California Institute of Technology, Pasadena, USA
D. Anderson, J. Bendavid, A. Bornheim, J. M. Lawhorn, H. B. Newman, T. Nguyen, C. Pena, M. Spiropulu, J. R. Vlimant, S. Xie, Z. Zhang, R. Y. Zhu

Carnegie Mellon University, Pittsburgh, USA
M. B. Andrews, T. Ferguson, M. Paulini, J. Russ, M. Sun, H. Vogel, I. Vorobiev, M. Weinberg

University of Colorado Boulder, Boulder, USA
J. P. Cumalat, W. T. Ford, F. Jensen, A. Johnson, M. Krohn, S. Leontsinis, T. Mulholland, K. Stenson, S. R. Wagner

Cornell University, Ithaca, USA
J. Alexander, J. Chaves, J. Chu, S. Dittmer, K. Mcdermott, N. Mirman, J. R. Patterson, A. Rinkevicius, A. Ryd, L. Skinnari, L. Soffi, S. M. Tan, Z. Tao, J. Thom, J. Tucker, P. Wittich, M. Zientek

Fairfield University, Fairfield, USA
D. Winn

Fermi National Accelerator Laboratory, Batavia, USA
S. Abdullin, M. Albrow, G. Apollinari, A. Apresyan, A. Apyan, S. Banerjee, L. A. T. Bauerdick, A. Beretvas, J. Berryhill, P. C. Bhat, G. Bolla, K. Burkett, J. N. Butler, A. Canepa, H. W. K. Cheung, F. Chlebana, M. Cremonesi, J. Duarte,

V. D. Elvira, I. Fisk, J. Freeman, Z. Gecse, E. Gottschalk, L. Gray, D. Green, S. Grünendahl, O. Gutsche, R. M. Harris, S. Hasegawa, J. Hirschauer, Z. Hu, B. Jayatilaka, S. Jindariani, M. Johnson, U. Joshi, B. Klima, B. Kreis, S. Lammel, D. Lincoln, R. Lipton, M. Liu, T. Liu, R. Lopes De Sá, J. Lykken, K. Maeshima, N. Magini, J. M. Marraffino, S. Maruyama, D. Mason, P. McBride, P. Merkel, S. Mrenna, S. Nahn, V. O'Dell, K. Pedro, O. Prokofyev, G. Rakness, L. Ristori, B. Schneider, E. Sexton-Kennedy, A. Soha, W. J. Spalding, L. Spiegel, S. Stoynev, J. Strait, N. Strobbe, L. Taylor, S. Tkaczyk, N. V. Tran, L. Uplegger, E. W. Vaandering, C. Vernieri, M. Verzocchi, R. Vidal, M. Wang, H. A. Weber, A. Whitbeck

University of Florida, Gainesville, USA
D. Acosta, P. Avery, P. Bortignon, A. Brinkerhoff, A. Carnes, M. Carver, D. Curry, S. Das, R. D. Field, I. K. Furic, J. Konigsberg, A. Korytov, K. Kotov, P. Ma, K. Matchev, H. Mei, G. Mitselmakher, D. Rank, D. Sperka, N. Terentyev, L. Thomas, J. Wang, S. Wang, J. Yelton

Florida International University, Miami, USA
S. Linn, P. Markowitz, G. Martinez, J. L. Rodriguez

Florida State University, Tallahassee, USA
A. Ackert, T. Adams, A. Askew, S. Hagopian, V. Hagopian, K. F. Johnson, T. Kolberg, T. Perry, H. Prosper, A. Santra, R. Yohay

Florida Institute of Technology, Melbourne, USA
M. M. Baarmand, V. Bhopatkar, S. Colafranceschi, M. Hohlmann, D. Noonan, T. Roy, F. Yumiceva

University of Illinois at Chicago (UIC), Chicago, USA
M. R. Adams, L. Apanasevich, D. Berry, R. R. Betts, R. Cavanaugh, X. Chen, O. Evdokimov, C. E. Gerber, D. A. Hangal, D. J. Hofman, K. Jung, J. Kamin, I. D. Sandoval Gonzalez, M. B. Tonjes, H. Trauger, N. Varelas, H. Wang, Z. Wu, J. Zhang

The University of Iowa, Iowa City, USA
B. Bilki[66], W. Clarida, K. Dilsiz[67], S. Durgut, R. P. Gandrajula, M. Haytmyradov, V. Khristenko, J.-P. Merlo, H. Mermerkaya[68], A. Mestvirishvili, A. Moeller, J. Nachtman, H. Ogul[69], Y. Onel, F. Ozok[70], A. Penzo, C. Snyder, E. Tiras, J. Wetzel, K. Yi

Johns Hopkins University, Baltimore, USA
B. Blumenfeld, A. Cocoros, N. Eminizer, D. Fehling, L. Feng, A. V. Gritsan, P. Maksimovic, J. Roskes, U. Sarica, M. Swartz, M. Xiao, C. You

The University of Kansas, Lawrence, USA
A. Al-bataineh, P. Baringer, A. Bean, S. Boren, J. Bowen, J. Castle, S. Khalil, A. Kropivnitskaya, D. Majumder, W. Mcbrayer, M. Murray, C. Royon, S. Sanders, E. Schmitz, R. Stringer, J. D. Tapia Takaki, Q. Wang

Kansas State University, Manhattan, USA
A. Ivanov, K. Kaadze, Y. Maravin, A. Mohammadi, L. K. Saini, N. Skhirtladze, S. Toda

Lawrence Livermore National Laboratory, Livermore, USA
F. Rebassoo, D. Wright

University of Maryland, College Park, USA
C. Anelli, A. Baden, O. Baron, A. Belloni, B. Calvert, S. C. Eno, C. Ferraioli, N. J. Hadley, S. Jabeen, G. Y. Jeng, R. G. Kellogg, J. Kunkle, A. C. Mignerey, F. Ricci-Tam, Y. H. Shin, A. Skuja, S. C. Tonwar

Massachusetts Institute of Technology, Cambridge, USA
D. Abercrombie, B. Allen, V. Azzolini, R. Barbieri, A. Baty, R. Bi, S. Brandt, W. Busza, I. A. Cali, M. D'Alfonso, Z. Demiragli, G. Gomez Ceballos, M. Goncharov, D. Hsu, Y. Iiyama, G. M. Innocenti, M. Klute, D. Kovalskyi, Y. S. Lai, Y.-J. Lee, A. Levin, P. D. Luckey, B. Maier, A. C. Marini, C. Mcginn, C. Mironov, S. Narayanan, X. Niu, C. Paus, C. Roland, G. Roland, J. Salfeld-Nebgen, G. S. F. Stephans, K. Tatar, D. Velicanu, J. Wang, T. W. Wang, B. Wyslouch

University of Minnesota, Minneapolis, USA
A. C. Benvenuti, R. M. Chatterjee, A. Evans, P. Hansen, S. Kalafut, S. C. Kao, Y. Kubota, Z. Lesko, J. Mans, S. Nourbakhsh, N. Ruckstuhl, R. Rusack, N. Tambe, J. Turkewitz

University of Mississippi, Oxford, USA

J. G. Acosta, S. Oliveros

University of Nebraska-Lincoln, Lincoln, USA

E. Avdeeva, K. Bloom, D. R. Claes, C. Fangmeier, R. Gonzalez Suarez, R. Kamalieddin, I. Kravchenko, J. Monroy,
J. E. Siado, G. R. Snow, B. Stieger

State University of New York at Buffalo, Buffalo, USA

M. Alyari, J. Dolen, A. Godshalk, C. Harrington, I. Iashvili, D. Nguyen, A. Parker, S. Rappoccio, B. Roozbahani

Northeastern University, Boston, USA

G. Alverson, E. Barberis, A. Hortiangtham, A. Massironi, D. M. Morse, D. Nash, T. Orimoto, R. Teixeira De Lima,
D. Trocino, R.-J. Wang, D. Wood

Northwestern University, Evanston, USA

S. Bhattacharya, O. Charaf, K. A. Hahn, N. Mucia, N. Odell, B. Pollack, M. H. Schmitt, K. Sung, M. Trovato, M. Velasco

University of Notre Dame, Notre Dame, USA

N. Dev, M. Hildreth, K. Hurtado Anampa, C. Jessop, D. J. Karmgard, N. Kellams, K. Lannon, N. Loukas, N. Marinelli,
F. Meng, C. Mueller, Y. Musienko[34], M. Planer, A. Reinsvold, R. Ruchti, N. Rupprecht, G. Smith, S. Taroni, M. Wayne,
M. Wolf, A. Woodard

The Ohio State University, Columbus, USA

J. Alimena, L. Antonelli, B. Bylsma, L. S. Durkin, S. Flowers, B. Francis, A. Hart, C. Hill, W. Ji, B. Liu, W. Luo,
D. Puigh, B. L. Winer, H. W. Wulsin

Princeton University, Princeton, USA

A. Benaglia, S. Cooperstein, O. Driga, P. Elmer, J. Hardenbrook, P. Hebda, D. Lange, J. Luo, D. Marlow, K. Mei,
I. Ojalvo, J. Olsen, C. Palmer, P. Piroué, D. Stickland, A. Svyatkovskiy, C. Tully

University of Puerto Rico, Mayaguez, USA

S. Malik

Purdue University, West Lafayette, USA

A. Barker, V. E. Barnes, S. Folgueras, L. Gutay, M. K. Jha, M. Jones, A. W. Jung, A. Khatiwada, D. H. Miller,
N. Neumeister, J. F. Schulte, J. Sun, F. Wang, W. Xie

Purdue University Northwest, Hammond, USA

T. Cheng, N. Parashar, J. Stupak

Rice University, Houston, USA

A. Adair, B. Akgun, Z. Chen, K. M. Ecklund, F. J. M. Geurts, M. Guilbaud, W. Li, B. Michlin, M. Northup, B. P. Padley,
J. Roberts, J. Rorie, Z. Tu, J. Zabel

University of Rochester, Rochester, USA

B. Betchart, A. Bodek, P. de Barbaro, R. Demina, Y. T. Duh, T. Ferbel, M. Galanti, A. Garcia-Bellido, J. Han,
O. Hindrichs, A. Khukhunaishvili, K. H. Lo, P. Tan, M. Verzetti

The Rockefeller University, New York, USA

R. Ciesielski, K. Goulianos, C. Mesropian

Rutgers, The State University of New Jersey, Piscataway, USA

A. Agapitos, J. P. Chou, Y. Gershtein, T. A. Gómez Espinosa, E. Halkiadakis, M. Heindl, E. Hughes, S. Kaplan,
R. Kunnawalkam Elayavalli, S. Kyriacou, A. Lath, R. Montalvo, K. Nash, M. Osherson, H. Saka, S. Salur, S. Schnetzer,
D. Sheffield, S. Somalwar, R. Stone, S. Thomas, P. Thomassen, M. Walker

University of Tennessee, Knoxville, USA

M. Foerster, J. Heideman, G. Riley, K. Rose, S. Spanier, K. Thapa

Texas A&M University, College Station, USA

O. Bouhali[71], A. Castaneda Hernandez[71], A. Celik, M. Dalchenko, M. De Mattia, A. Delgado, S. Dildick, R. Eusebi,

J. Gilmore, T. Huang, T. Kamon[72], R. Mueller, Y. Pakhotin, R. Patel, A. Perloff, L. Perniè, D. Rathjens, A. Safonov, A. Tatarinov, K. A. Ulmer

Texas Tech University, Lubbock, USA
N. Akchurin, J. Damgov, F. De Guio, C. Dragoiu, P. R. Dudero, J. Faulkner, E. Gurpinar, S. Kunori, K. Lamichhane, S. W. Lee, T. Libeiro, T. Peltola, S. Undleeb, I. Volobouev, Z. Wang

Vanderbilt University, Nashville, USA
S. Greene, A. Gurrola, R. Janjam, W. Johns, C. Maguire, A. Melo, H. Ni, P. Sheldon, S. Tuo, J. Velkovska, Q. Xu

University of Virginia, Charlottesville, USA
M. W. Arenton, P. Barria, B. Cox, R. Hirosky, A. Ledovskoy, H. Li, C. Neu, T. Sinthuprasith, X. Sun, Y. Wang, E. Wolfe, F. Xia

Wayne State University, Detroit, USA
C. Clarke, R. Harr, P. E. Karchin, J. Sturdy, S. Zaleski

University of Wisconsin-Madison, Madison, WI, USA
D. A. Belknap, J. Buchanan, C. Caillol, S. Dasu, L. Dodd, S. Duric, B. Gomber, M. Grothe, M. Herndon, A. Hervé, U. Hussain, P. Klabbers, A. Lanaro, A. Levine, K. Long, R. Loveless, G. A. Pierro, G. Polese, T. Ruggles, A. Savin, N. Smith, W. H. Smith, D. Taylor, N. Woods

1: Also at Vienna University of Technology, Vienna, Austria
2: Also at State Key Laboratory of Nuclear Physics and Technology, Peking University, Beijing, China
3: Also at Universidade Estadual de Campinas, Campinas, Brazil
4: Also at Universidade Federal de Pelotas, Pelotas, Brazil
5: Also at Université Libre de Bruxelles, Brussels, Belgium
6: Also at Joint Institute for Nuclear Research, Dubna, Russia
7: Now at Ain Shams University, Cairo, Egypt
8: Now at British University in Egypt, Cairo, Egypt
9: Now at Cairo University, Cairo, Egypt
10: Also at Université de Haute Alsace, Mulhouse, France
11: Also at Skobeltsyn Institute of Nuclear Physics, Lomonosov Moscow State University, Moscow, Russia
12: Also at CERN, European Organization for Nuclear Research, Geneva, Switzerland
13: Also at RWTH Aachen University, III. Physikalisches Institut A, Aachen, Germany
14: Also at University of Hamburg, Hamburg, Germany
15: Also at Brandenburg University of Technology, Cottbus, Germany
16: Also at Institute of Nuclear Research ATOMKI, Debrecen, Hungary
17: Also at MTA-ELTE Lendület CMS Particle and Nuclear Physics Group, Eötvös Loránd University, Budapest, Hungary
18: Also at Institute of Physics, University of Debrecen, Debrecen, Hungary
19: Also at Indian Institute of Technology Bhubaneswar, Bhubaneswar, India
20: Also at Institute of Physics, Bhubaneswar, India
21: Also at University of Visva-Bharati, Santiniketan, India
22: Also at University of Ruhuna, Matara, Sri Lanka
23: Also at Isfahan University of Technology, Isfahan, Iran
24: Also at Yazd University, Yazd, Iran
25: Also at Plasma Physics Research Center, Science and Research Branch, Islamic Azad University, Tehran, Iran
26: Also at Università degli Studi di Siena, Siena, Italy
27: Also at INFN Sezione di Milano-Bicocca; Università di Milano-Bicocca, Milan, Italy
28: Also at Laboratori Nazionali di Legnaro dell'INFN, Legnaro, Italy
29: Also at Purdue University, West Lafayette, USA
30: Also at International Islamic University of Malaysia, Kuala Lumpur, Malaysia
31: Also at Malaysian Nuclear Agency, MOSTI, Kajang, Malaysia
32: Also at Consejo Nacional de Ciencia y Tecnología, Mexico city, Mexico
33: Also at Warsaw University of Technology, Institute of Electronic Systems, Warsaw, Poland
34: Also at Institute for Nuclear Research, Moscow, Russia

35: Now at National Research Nuclear University 'Moscow Engineering Physics Institute' (MEPhI), Moscow, Russia

36: Also at Institute of Nuclear Physics of the Uzbekistan Academy of Sciences, Tashkent, Uzbekistan

37: Also at St. Petersburg State Polytechnical University, St. Petersburg, Russia

38: Also at University of Florida, Gainesville, USA

39: Also at P.N. Lebedev Physical Institute, Moscow, Russia

40: Also at California Institute of Technology, Pasadena, USA

41: Also at Budker Institute of Nuclear Physics, Novosibirsk, Russia

42: Also at Faculty of Physics, University of Belgrade, Belgrade, Serbia

43: Also at INFN Sezione di Roma; Sapienza Università di Roma, Rome, Italy

44: Also at University of Belgrade, Faculty of Physics and Vinca Institute of Nuclear Sciences, Belgrade, Serbia

45: Also at Scuola Normale e Sezione dell'INFN, Pisa, Italy

46: Also at National and Kapodistrian University of Athens, Athens, Greece

47: Also at Riga Technical University, Riga, Latvia

48: Also at Institute for Theoretical and Experimental Physics, Moscow, Russia

49: Also at Albert Einstein Center for Fundamental Physics, Bern, Switzerland

50: Also at Istanbul University, Faculty of Science, Istanbul, Turkey

51: Also at Adiyaman University, Adiyaman, Turkey

52: Also at Istanbul Aydin University, Istanbul, Turkey

53: Also at Mersin University, Mersin, Turkey

54: Also at Cag University, Mersin, Turkey

55: Also at Piri Reis University, Istanbul, Turkey

56: Also at Gaziosmanpasa University, Tokat, Turkey

57: Also at Izmir Institute of Technology, Izmir, Turkey

58: Also at Necmettin Erbakan University, Konya, Turkey

59: Also at Marmara University, Istanbul, Turkey

60: Also at Kafkas University, Kars, Turkey

61: Also at Istanbul Bilgi University, Istanbul, Turkey

62: Also at Rutherford Appleton Laboratory, Didcot, UK

63: Also at School of Physics and Astronomy, University of Southampton, Southampton, UK

64: Also at Instituto de Astrofísica de Canarias, La Laguna, Spain

65: Also at Utah Valley University, Orem, USA

66: Also at Beykent University, Istanbul, Turkey

67: Also at Bingol University, Bingol, Turkey

68: Also at Erzincan University, Erzincan, Turkey

69: Also at Sinop University, Sinop, Turkey

70: Also at Mimar Sinan University, Istanbul, Istanbul, Turkey

71: Also at Texas A&M University at Qatar, Doha, Qatar

72: Also at Kyungpook National University, Daegu, Korea